Production rates of hidden-charm pentaquark molecules in Λ_b decays

Ya-Wen Pan,[1] Ming-Zhu Liu,[2,1,*] and Li-Sheng Geng[1,3,4,5,†]

[1]*School of Physics, Beihang University, Beijing 102206, China*
[2]*School of Nuclear Science and Technology, Lanzhou University, Lanzhou 730000, China*
[3]*Beijing Key Laboratory of Advanced Nuclear Materials and Physics, Beihang University, Beijing 102206, China*
[4]*Peng Huanwu Collaborative Center for Research and Education, Beihang University, Beijing 100191, China*
[5]*Southern Center for Nuclear-Science Theory (SCNT), Institute of Modern Physics, Chinese Academy of Sciences, Huizhou 516000, China*

(Received 9 October 2023; accepted 16 November 2023; published 18 December 2023)

The partial decay widths and production mechanism of the three pentaquark states, $P_\psi^N(4312)$, $P_\psi^N(4440)$, and $P_\psi^N(4457)$, discovered by the LHCb Collaboration in 2019, are still under debate. In this work, we employ the contact-range effective field theory approach to construct the $\bar{D}^{(*)}\Sigma_c^{(*)}$, $\bar{D}^*\Lambda_c$, $\bar{D}\Lambda_c$, $J/\psi p$, and $\eta_c p$ coupled-channel interactions to dynamically generate the multiplet of hidden-charm pentaquark molecules by reproducing the masses and widths of $P_\psi^N(4312)$, $P_\psi^N(4440)$, and $P_\psi^N(4457)$. Assuming that the pentaquark molecules are produced in the Λ_b decay via the triangle diagrams, where Λ_b first decays into $D_s^{(*)}\Lambda_c$, then $D_s^{(*)}$ scatters into $\bar{D}^{(*)}K$, and finally the molecules are dynamically generated by the $\bar{D}^{(*)}\Lambda_c$ interactions, we calculate the branching fractions of the decays $\Lambda_b \to P_\psi^N K$ using the effective Lagrangian approach. With the partial decay widths of these pentaquark molecules, we further estimate the branching fractions of the decays $\Lambda_b \to (P_\psi^N \to J/\psi p)K$ and $\Lambda_b \to (P_\psi^N \to \bar{D}^*\Lambda_c)K$. Our results show that the pentaquark states $P_\psi^N(4312)$, $P_\psi^N(4440)$, and $P_\psi^N(4457)$ as hadronic molecules can be produced in the Λ_b decay, and on the other hand their heavy quark spin symmetry partners are invisible in the $J/\psi p$ invariant mass distribution because of the small production rates. Our studies show that it is possible to observe some of the pentaquark states in the $\Lambda_b \to \bar{D}^*\Lambda_c K$ decays.

DOI: 10.1103/PhysRevD.108.114022

I. INTRODUCTION

In 2015, two pentaquark states $P_\psi^N(4380)$ and $P_\psi^N(4450)$ were observed by the LHCb Collaboration in the $J/\psi p$ invariant mass distributions of the $\Lambda_b \to J/\psi p K$ decay [1]. Four years later, they updated the data sample and found that the original $P_\psi^N(4450)$ state splits into two states, $P_\psi^N(4440)$ and $P_\psi^N(4457)$, and a new state $P_\psi^N(4312)$ emerges below the $\bar{D}\Sigma_c$ threshold [2]. Recently the LHCb Collaboration found the evidence for the hidden-charm pentaquark state $P_\psi^N(4337)$ in the B_s meson decay [3], as well as the hidden-charm pentaquark states with strangeness $P_{\psi s}^\Lambda(4459)$ in the Ξ_b decay [4], the existence of which needs to be confirmed because at present the significance of the observation is only about 3σ. Very recently the LHCb Collaboration reported another pentaquark state $P_{\psi s}^\Lambda(4338)$ in the B decay with a high significance [5]. In this work, we only focus on the three pentaquark states $P_\psi^N(4312)$, $P_\psi^N(4440)$, and $P_\psi^N(4457)$, which have been extensively studied in a series of theoretical works. We note that although the $\bar{D}^{(*)}\Sigma_c$ molecular interpretations for these pentaquark states are the most popular [6–23], there exist other explanations, e.g., hadrocharmonia [24], compact pentaquark states [25–31], virtual states [32], triangle singularities [33], and cusp effects [34].

From the perspective of masses, the three pentaquark states can be nicely arranged into the $\bar{D}^{(*)}\Sigma_c^{(*)}$ multiplet. However, their widths obtained in the hadronic molecular picture always deviate a bit from the experimental data. In Ref. [35], we found that their partial decay widths into three-body final states $\bar{D}^{(*)}\Lambda_c\pi$ are only at the order of a few hundreds of keV, which indicates that the two-body decay modes are dominant. The chiral unitary study found that the partial decay widths of $P_\psi^N \to J/\psi p(\eta_c p)$ account

*zhengmz11@buaa.edu.cn
†lisheng.geng@buaa.edu.cn

for the largest portion of their total decay widths [9], while the study based on the triangle diagrams shows that the three P_ψ^N states mainly decay into $\bar{D}^{(*)}\Lambda_c$ [36]. In Refs. [11,12,37], the authors argued that the one-pion exchange is responsible for the $\bar{D}^{(*)}\Sigma_c \to \bar{D}^{(*)}\Lambda_c$ interactions, and therefore dominantly contributes to the widths of the pentaquark states. From these studies, we conclude that these three molecules mainly decay via two modes: hidden-charm $J/\psi p(\eta_c p)$ and open-charm $\bar{D}^{(*)}\Lambda_c$. Considering the upper limit of the branching fraction $\mathcal{B}(P_\psi^N \to J/\psi p) < 2\%$ measured in the photoproduction processes [38,39], the partial decays $P_\psi^N \to \bar{D}^{(*)}\Lambda_c$ are expected to play a dominant role. However, such small upper limits cannot be easily reconciled with the current LHCb data [40]. In this work, we employ the contact-range effective field theory(EFT) approach to revisit the partial decay widths of the hidden-charm pentaquark molecules by studying their two- and three-body decays.

Up to now, the hidden-charm pentaquark states have only been observed in the exclusive b decays in proton-proton collisions. The productions of pentaquark states in other processes have been proposed. In Refs. [41–45], the authors claimed that the hidden-charm pentaquark states can be produced in the J/ψ photoproduction off proton. This process could distinguish whether these pentaquark states are genuine states or anomalous triangle singularities. Moreover, it is suggested that the hidden-charm pentaquark states can be produced in the e^+e^- collisions [46] and antiproton-deuteron collisions [47]. Based on Monte Carlo simulations, the inclusive production rates of these pentaquark states are estimated in proton-proton collisions 48,49]] and electron-proton collisions [50], which are helpful for future experimental searches for the pentaquark states. In this work, based on the LHCb data, we primarily focus on the production mechanism of the pentaquark states in the Λ_b decays.

The production mechanism of the pentaquark states in the Λ_b decays can be classified into two categories. In mechanism I, the mother particle M weakly decays into three particles A, B, and C, and the hadronic molecule under study can be dynamically generated via the rescattering of any two particles of A, B, and C. This mechanism has already been applied to study the production rates of $X(3872)$ as a $\bar{D}D^*$ molecule via the weak decays $B \to \bar{D}D^*K$ [51,52]. For the pentaquark states, it was proposed that the weak decays of $\Lambda_b \to \bar{D}^{(*)}\Sigma_c K$ and $\Lambda_b \to J/\psi p K$ can dynamically generate the hidden-charm pentaquark molecules via the $\bar{D}^{(*)}\Sigma_c$ rescattering [16,53] and $J/\psi p$ rescatterring [54], respectively, which can well describe the experimental invariant mass distribution of $J/\psi p$, while their absolute production rates are not quantitatively estimated. In particular, as pointed out in Ref. [34], the branching fractions $\mathrm{Br}(\Lambda_b \to \bar{D}^{(*)}\Sigma_c K)$ are so tiny that the pentaquark molecules are rather difficult to be produced via the weak decays $\Lambda_b \to \bar{D}^{(*)}\Sigma_c K$. Therefore, whether these pentaquark molecules can be produced via Mechanism I remains unsettled.

In Mechanism II, the mother particle M weakly decays into two states A and B, then A scatters (or decays) into C and D, and finally the final-state interaction of B and C dynamically generates the molecules of interest [55–59]. A typical example is that the $X(3872)$ as a $\bar{D}D^*$ molecule can be generated through the weak decays $B \to \bar{D}^{(*)}D_s^{(*)}$ following $D_s^{(*)}$ scattering into $D^{(*)}K$ [59]. In Ref. [60], Wu *et al.* proposed that Λ_b weakly decays into Σ_c and $D_s^{(*)}$, then $D_s^{(*)}$ scatter into $\bar{D}^{(*)}$ and K, and the pentaquark molecules are finally generated via the $\bar{D}^{(*)}\Sigma_c$ interactions. We note that the Λ_b decaying into $\Sigma_c^{(*)}$ is highly suppressed due to the fact the light quark pair transition between a symmetric and antisymmetric spin-flavor configuration is forbidden [61,62], which indicates that the production of pentaquark molecules is difficult (if not impossible) via the weak decays of $\Lambda_b \to D_s^{(*)}\Sigma_c$.[1] In Ref. [34], the authors select the color favorable weak decays $\Lambda_b \to D_s^{(*)}\Lambda_c$ to produce the pentaquark molecules as well as to analyze their mass distributions, but did not explicitly calculate their productions rates. Following Refs. [58,59], we take the effective Lagrangian approach to calculate the production rates of the pentaquark molecules in Λ_b decays with no free parameters, and try to answer the questions whether the three pentaquark states $P_\psi^N(4312)$, $P_\psi^N(4440)$, and $P_\psi^N(4457)$ as hadronic molecules can be produced in the Λ_b decays, as well as why their HQSS partners have not been observed in the same decays.

This work is organized as follows. We first calculate the two-body partial decay widths of the pentaquark molecules obtained by the contact range EFT, and the amplitudes of their production mechanism in Λ_b decays via the triangle diagrams using the effective Lagrangian approach in Sec. II. The results and discussions on the widths of the pentaquark molecules and the branching fractions of the decays $P_\psi^N \to J/\psi p$ and $P_\psi^N \to \bar{D}^{(*)}\Lambda_c$, as well as the branching fractions of the weak decays $\Lambda_b \to P_\psi^N K$, $\Lambda_b \to (P_\psi^N \to J/\psi p)K$, and $\Lambda_b \to (P_\psi^N \to \bar{D}^*\Lambda_c)K$ are provided in Sec. III, followed by a short summary in the last section.

II. THEORETICAL FRAMEWORK

In this work, we employ the triangle diagrams to describe the productions of pentaquark molecules. We suppose that the color favored weak decays $\Lambda_b \to \Lambda_c D_s^{(*)-}$ are responsible for the short-range interactions because the

[1] In Ref. [60], the $\Lambda_b \to \Sigma_c$ transition is assumed to be proportional to the $\Lambda_b \to \Lambda_c$ transition, characterized by an unknown parameter R. By reproducing the experimental production rates of the pentaquark molecules, R is found to be about 0.1.

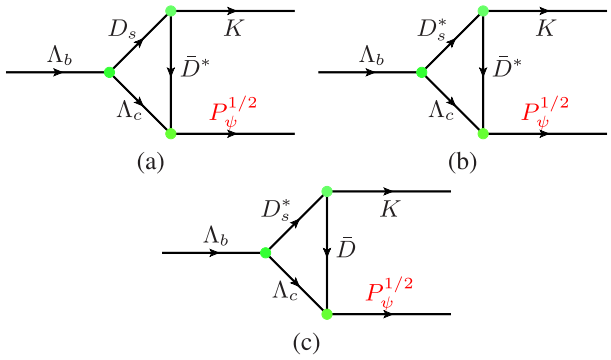

FIG. 1. Triangle diagrams accounting for $\Lambda_b \to D_s^{(*)}\Lambda_c \to P_\psi^{1/2}K$ with $P_\psi^{1/2}$ representing one of the pentaquark molecules of spin $1/2$.

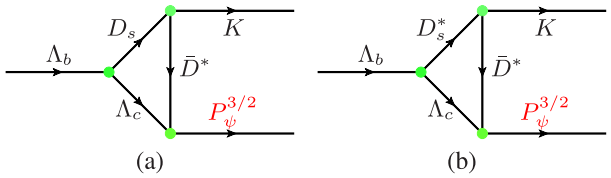

FIG. 2. Triangle diagrams accounting for $\Lambda_b \to D_s^{(*)}\Lambda_c \to P_\psi^{3/2}K$ with $P_\psi^{3/2}$ denoting one of the pentaquark molecule of spin $3/2$.

branching fractions $\mathcal{B}(\Lambda_b \to \Lambda_c D_s^{(*)-})$ are large among the nonleptonic decays of Λ_b. Then the $D_s^{(*)-}$ mesons scatter into $\bar{D}^{(*)}$ and K mesons, and the pentaquark molecules with spin $1/2$ and $3/2$ are dynamically generated via the $\bar{D}^{(*)}\Lambda_c$ interactions as shown in Figs. 1 and 2, respectively, where $P_\psi^{1/2}$ and $P_\psi^{3/2}$ denote the pentaquark molecules of spin $1/2$ and $3/2$, respectively. As shown in a number of previous studies [9,11,12,16,18,21,63–66] and also explicitly shown later, there exists a complete multiplet of hidden-charm pentaquark molecules dominantly generated by the $\bar{D}^{(*)}\Sigma_c^{(*)}$ interactions. We denote the seven pentaquark molecules as $P_{\psi 1}^N, P_{\psi 2}^N, \ldots, P_{\psi 7}^N$, following the order of scenario A of Table I in Ref. [63]. It should be noted that such order specifies the spin of pentaquark molecules, i.e., $P_{\psi 3}^N$ and $P_{\psi 4}^N$ represent the pentaquark molecules of spin $1/2$ and $3/2$, respectively. In this work, we study two scenarios A and B corresponding to different spin assignments of these pentaquark molecules. In scenario A, $P_{\psi 3}^N$ and $P_{\psi 4}^N$ represent $P_\psi^N(4440)$ and $P_\psi^N(4457)$, while they represent $P_\psi^N(4457)$ and $P_\psi^N(4440)$ in scenario B. $P_{\psi 1}^N$ represents $P_\psi^N(4312)$ in both scenario A and scenario B. Considering only S-wave $\bar{D}^{(*)}\Lambda_c$ interactions, the production of the pentaquark molecule of spin $5/2$ is not allowed by the mechanisms shown in either Fig. 1 or 2, which indicate that $P_{\psi 7}^N$ cannot be produced in our model. Therefore, we only focus on the productions of the remaining six pentaquark molecules in the Λ_b decays in this work.

A. Effective Lagrangians

In this work, we adopt the effective Lagrangian approach to calculate the triangle diagrams of Figs. 1 and 2. In the following, we spell out the relevant Lagrangians.

First, we focus on the weak decays of $\Lambda_b \to \Lambda_c D_s^{(*)-}$. At quark level, the decays of $\Lambda_b \to \Lambda_c D_s^{(*)-}$ can occur via the external W-emission mechanism shown in Fig. 3, which is usually the largest in terms of the topological classification of weak decays [67–69]. As shown in Ref. [59], the color favored weak decays $B \to D_s^{(*)}D^{(*)}$ are significant to produce the $\bar{D}^*D^{(*)}$ molecules in B decays, which share similar topologies to the weak decays $\Lambda_b \to \Lambda_c D_s^{(*)-}$ at quark level.

The effective Hamiltonian describing the weak decays of $\Lambda_b \to \Lambda_c D_s^{(*)-}$ has the following form

$$\mathcal{H}_{\text{eff}} = \frac{G_F}{\sqrt{2}} V_{cb}V_{cs}[c_1(\mu)\mathcal{O}_1(\mu) + c_2(\mu)\mathcal{O}_2(\mu)] + \text{H.c.} \quad (1)$$

where G_F is the Fermi constant, V_{bc} and V_{cs} are the Cabibbo-Kobayashi-Maskawa (CKM) matrix elements, $c_{1,2}(\mu)$ are the Wilson coefficients, and $\mathcal{O}_1(\mu)$ and $\mathcal{O}_2(\mu)$ are the four-fermion operators of $(s\bar{c})_{V-A}(c\bar{b})_{V-A}$ and $(\bar{c}c)_{V-A}(s\bar{b})_{V-A}$ with $(\bar{q}q)_{V-A}$ standing for $\bar{q}\gamma_\mu(1-\gamma_5)q$ [70–72]. The Wilson coefficients $c_{1,2}(\mu)$ include the short-distance quantum chromodynamics (QCD) dynamic scaling from $\mu = M_W$ to $\mu = m_c$.

In the naive factorization approach [73], the amplitudes of $\Lambda_b \to \Lambda_c D_s^{(*)-}$ can be expressed as the products of two current hadronic matrix elements

$$\mathcal{A}(\Lambda_b \to \Lambda_c D_s^-) = \frac{G_F}{\sqrt{2}} V_{cb}V_{cs}a_1\langle D_s^-|(s\bar{c})|0\rangle\langle\Lambda_c|(c\bar{b})|\Lambda_b\rangle \quad (2)$$

$$\mathcal{A}(\Lambda_b \to \Lambda_c D_s^{*-}) = \frac{G_F}{\sqrt{2}} V_{cb}V_{cs}a_1\langle D_s^{*-}|(s\bar{c})|0\rangle\langle\Lambda_c|(c\bar{b})|\Lambda_b\rangle \quad (3)$$

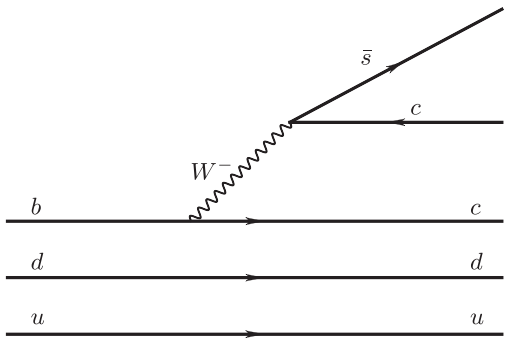

FIG. 3. External W-emission accounting for $\Lambda_b \to D_s^{(*)}\Lambda_c$ at quark level.

where the effective Wilson coefficient a_1 is expressed as $a_1 = c_1(\mu) + c_2(\mu)/N_c$ with $N_c = 3$ the number of colors [72,73].

The matrix elements between a pseudoscalar meson or vector meson and the vacuum have the following form:

$$\langle D_s^-|(s\bar{c})|0\rangle = if_{D_s^-}p^\mu_{D_s^-}, \tag{4}$$

$$\langle D_s^{*-}|(s\bar{c})|0\rangle = m_{D_s^{*-}}f_{D_s^{*-}}\epsilon^*_\mu, \tag{5}$$

where $f_{D_s^-}$ and $f_{D_s^{*-}}$ are the decay constants for D_s^- and D_s^{*-}, respectively, and ϵ^*_μ denotes the polarization vector of D_s^{*-}.

The $\Lambda_b \to \Lambda_c$ transition form factors are parametrized as follows [62]

$$\begin{aligned}&\langle B(p')|V_\mu - A_\mu|B(p)\rangle \\ &= \bar{u}(p')\left[f_1^V(q^2)\gamma_\mu - f_2^V(q^2)\frac{i\sigma_{\mu\nu}q^\nu}{m} + f_3^V(q^2)\frac{q^\mu}{m}\right. \\ &\left. - \left(f_1^A(q^2)\gamma_\mu - f_2^A(q^2)\frac{i\sigma_{\mu\nu}q^\nu}{m} + f_3^A(q^2)\frac{q^\mu}{m}\right)\gamma^5\right]u(p)\end{aligned} \tag{6}$$

where $\sigma^{\mu\nu} = \frac{i}{2}(\gamma^\mu\gamma^\nu - \gamma^\nu\gamma^\mu)$ and $q = p - p'$. As a result, the weak decays $\Lambda_b \to \Lambda_c D_s^{(*)}$ can be characterized by the following Lagrangian [70]:

$$\begin{aligned}\mathcal{L}_{\Lambda_b\Lambda_c D_s} &= i\bar{\Lambda}_c(A + B\gamma_5)\Lambda_b D_s, \\ \mathcal{L}_{\Lambda_b\Lambda_c D_s^*} &= \bar{\Lambda}_c\left(A_1\gamma_\mu\gamma_5 + A_2\frac{p_{2\mu}}{m}\gamma_5 + B_1\gamma_\mu + B_2\frac{p_{2\mu}}{m}\right)\Lambda_b D_s^{*\mu},\end{aligned} \tag{7}$$

where A_1, A_2, B_1, B_2, A, and B are

$$\begin{aligned}A &= \lambda f_{D_s}\left[(m - m_2)f_1^V + \frac{m_1^2}{m}f_3^V\right], \\ B &= \lambda f_{D_s}\left[(m + m_2)f_1^A - \frac{m_1^2}{m}f_3^A\right], \\ A_1 &= -\lambda f_{D_s^*}m_1\left[f_1^A - f_2^A\frac{m - m_2}{m}\right], \\ B_1 &= \lambda f_{D_s^*}m_1\left[f_1^V + f_2^V\frac{m + m_2}{m}\right], \\ A_2 &= 2\lambda f_{D_s^*}m_1 f_2^A, \\ B_2 &= -2\lambda f_{D_s^*}m_1 f_2^V.\end{aligned} \tag{8}$$

with $\lambda = \frac{G_F}{\sqrt{2}}V_{cb}V_{cs}a_1$ and m, m_1, m_2 referring to the masses of Λ_b, $D_s^{(*)}$, and Λ_c, respectively. The form factors can be expressed in a double-pole form:

$$f_i^{V/A}(q^2) = F_i^{V/A}(0)\frac{F_0}{1 - a\varphi + b\varphi^2} \tag{9}$$

TABLE I. Values of $F(0)$, a, b in the $\Lambda_b \to \Lambda_c$ transition form factors [74].

	F_1^V	F_2^V	F_3^V	F_1^A	F_2^A	F_3^A
$F(0)$	0.549	0.110	−0.023	0.542	0.018	−0.123
a	1.459	1.680	1.181	1.443	0.921	1.714
b	0.571	0.794	0.276	0.559	0.255	0.828

with $\varphi = q^2/m^2$. The values of F_0, a and b in the $\Lambda_b \to \Lambda_c$ transition form factors are taken from Ref. [74] and shown in Table I.

In this work, we take $G_F = 1.166 \times 10^{-5}$ GeV^{-2}, $V_{cb} = 0.041$, $V_{cs} = 0.987$, $f_{D_s^-} = 250$ MeV, and $f_{D_s^{*-}} = 272$ MeV as in Refs. [62,75–77]. We note that the value of a_1 as a function of the energy scale μ differs from process to process [78,79]. Therefore, we take the branching fraction $\mathcal{B}(\Lambda_b \to \Lambda_c D_s^-) = (1.10 \pm 0.10)\%$ to determine the effective Wilson coefficient to be $a_1 = 0.883$. We note that in Ref. [59], the effective Wilson coefficient a_1 are determined to be 0.79 and 0.81 by reproducing the branching fractions of the decays $B^+ \to \bar{D}^0 D_s^+$ and $B^+ \to \bar{D}^0 D_s^{*+}$, respectively. These values are consistent with the value obtained from the weak decay $\Lambda_b \to \Lambda_c D_s^-$, showing that the naive factorization approach works well for the external W-emission mechanism. Due to the nonavailability of experimental data for the branching fraction $\mathcal{B}(\Lambda_b \to \Lambda_c D_s^{*-})$, we assume that the effective Wilson coefficient in Eq. (3) is the same as that in Eq. (2). With the so obtained effective Wilson coefficient a_1 we predict the branching fraction $\mathcal{B}(\Lambda_b \to \Lambda_c D_s^{*-}) = (2.47 \pm 0.26)\%$, consistent with the results of Refs. [62,80]. As a matter of fact, the experimental branching fraction $\mathcal{B}(\Lambda_b \to \Lambda_c D_s^-)$ helps reduce the uncertainty in the weak vertices.

The Lagrangians describing the $D_s^{(*)}$ mesons scattering into $\bar{D}^{(*)}$ and K mesons are

$$\begin{aligned}\mathcal{L}_{KD_sD^*} &= ig_{KD_sD^*}D^{*\mu}[\bar{D}_s\partial_\mu K - (\partial_\mu\bar{D}_s)K] + \text{H.c.} \\ \mathcal{L}_{KD_s^*D^*} &= -g_{KD_s^*D^*}\epsilon^{\mu\nu\alpha\beta}[\partial_\mu\bar{D}^*_\nu\partial_\alpha D^*_{s\beta}\bar{K} \\ &\quad + \partial_\mu D^*_\nu\partial_\alpha\bar{D}^*_{s\beta}K] + \text{H.c.}\end{aligned} \tag{10}$$

where $g_{KD_sD^*}$ and $g_{KD_s^*D^*}$ are the kaon couplings to D_sD^* and $D_s^*D^*$, respectively. Unfortunately, there exists no experimental data to determine the values of these couplings. The coupling $g_{D_sD^*K}$ is estimated to be 16.6 and 10 assuming SU(3)-flavor symmetry [81] and SU(4)-flavor symmetry [82], respectively, while the QCD sum rule yields 5 [83,84]. In view of this large variance, we adopt the couplings estimated by SU(4) symmetry, which are in between those estimated utilizing SU(3) symmetry and by the QCD sum rule, i.e., $g_{D_sD^*K} = g_{D_s^*DK} = 10$ and $g_{D_s^*D^*K} = 7.0$ GeV^{-1} [82].

The effective Lagrangians describing the interactions between pentaquark molecules and their constituents $\bar{D}^{(*)}\Lambda_c$ are written as

$$\begin{aligned}\mathcal{L}_{P_\psi^{1/2}\Lambda_c\bar{D}} &= g_{P_\psi^{1/2}\Lambda_c\bar{D}} P_\psi^{1/2}\Lambda_c\bar{D},\\ \mathcal{L}_{P_\psi^{1/2}\Lambda_c\bar{D}^*} &= g_{P_\psi^{1/2}\Lambda_c\bar{D}^*}\bar{\Lambda}_c\gamma_5\left(g_{\mu\nu}-\frac{p_\mu p_\nu}{m^2_{P_\psi^{1/2}}}\right)\gamma^\nu P_\psi^{1/2}D^{*\mu},\\ \mathcal{L}_{P_\psi^{3/2}\Lambda_c\bar{D}^*} &= g_{P_\psi^{3/2}\Lambda_c\bar{D}^*}\bar{\Lambda}_c P^{3/2}_{\psi\mu}D^{*\mu},\end{aligned} \tag{11}$$

where $g_{P_\psi^{1/2}\Lambda_c\bar{D}}$, $g_{P_\psi^{1/2}\Lambda_c\bar{D}^*}$, and $g_{P_\psi^{3/2}\Lambda_c\bar{D}^*}$ are the couplings of the $P_\psi^{1/2}$ and $P_\psi^{3/2}$ pentaquark molecules to their constituents $\bar{D}^{(*)}\Lambda_c$. One should note that although these pentaquark molecules are dominantly generated by the $\bar{D}^{(*)}\Sigma_c^{(*)}$ interactions [63], the $\bar{D}^{(*)}\Lambda_c$ and $J/\psi(\eta_c)p$ coupled channels also play a relevant role [9,11,12,37,65,85]. Below, we estimate the couplings of the pentaquark molecules to their constituents $\bar{D}^{(*)}\Lambda_c$ and $J/\psi(\eta_c)p$ by the contact range EFT approach, which is widely applied to study the dynamical generation of hadronic molecules [22,86].

B. Contact-range EFT approach

In this subsection, we introduce the contact-range EFT approach. The scattering amplitude T is responsible for the dynamical generation of the pentaquark molecules via the Lippmann-Schwinger equation

$$T(\sqrt{s}) = (1 - VG(\sqrt{s}))^{-1}V, \tag{12}$$

where V is the coupled-channel potential determined by the contact-range EFT approach (see Appendix A), and $G(\sqrt{s})$ is the two-body propagator. In this work, we consider the following coupled channels $\bar{D}^*\Sigma_c^* - \bar{D}^*\Sigma_c - \bar{D}\Sigma_c - \bar{D}^*\Lambda_c - \bar{D}\Lambda_c - J/\psi p - \eta_c p$ with $J^P = 1/2^-$ and $\bar{D}^*\Sigma_c^* - \bar{D}^*\Sigma_c - \bar{D}^*\Lambda_c - J/\psi p$ with $J^P = 3/2^-$. Since the mass splitting between $\bar{D}^*\Sigma_c^*$ and $\eta_c p$ is about 600 MeV, we take a relativistic propagator:

$$G(\sqrt{s}) = 2m_1\int\frac{d^3q}{(2\pi)^3}\frac{\omega_1+\omega_2}{2\omega_1\omega_2}\frac{F(q^2,k)}{(\sqrt{s})^2-(\omega_1+\omega_2)^2+i\varepsilon} \tag{13}$$

where $\sqrt{s}$ is the total energy in the center-of-mass (c.m.) frame of m_1 and m_2, $\omega_i = \sqrt{m_i^2+q^2}$ is the energy of the particle and the c.m. momentum k is

$$k(\sqrt{s}) = \frac{\sqrt{\sqrt{s}^2-(m_1+m_2)^2}\sqrt{\sqrt{s}^2-(m_1-m_2)^2}}{2\sqrt{s}}. \tag{14}$$

A regulator of Gaussian form $F(q^2,k) = e^{-2q^2/\Lambda^2}/e^{-2k^2/\Lambda^2}$ is used to regulate the loop function. We note that the loop function can also be regularized by other methods such as the momentum cut off scheme and dimensional regularization scheme [87–91].

The dynamically generated pentaquark molecules correspond to poles on the unphysical sheet, which is defined as [92,93],

$$G_{II}(\sqrt{s}) = G_I(\sqrt{s}) + i\frac{2m_1}{4\pi}\frac{k(\sqrt{s})}{\sqrt{s}}, \tag{15}$$

where m_1 stands for the mass of the baryon.

With the potentials obtained in Eqs. (A6) and (A7) of Appendix A, we search for poles in the vicinity of the $\bar{D}^{(*)}\Sigma_c^{(*)}$ channels, and then determine the couplings between the pentaquark molecules and their constituents from the residues of the corresponding poles,

$$g_i g_j = \lim_{\sqrt{s}\to\sqrt{s_0}}(\sqrt{s}-\sqrt{s_0})T_{ij}(\sqrt{s}), \tag{16}$$

where g_i denotes the coupling of channel i to the dynamically generated molecules and $\sqrt{s_0}$ is the pole position.

Using the couplings g_i obtained above, one can estimate the partial decay widths of the pentaquark molecules [94]

$$\Gamma_i = g_i^2\frac{1}{2\pi}\frac{m_i}{m_{P_\psi^N}}p_i \tag{17}$$

where m_i stands for the mass of the baryon of channel i, $m_{P_\psi^N}$ is the mass of the pentaquark molecule (the real part of the pole position), and p_i is the momentum of the baryon (meson) of channel i in the P_ψ^N rest frame.

C. Decay amplitudes

With the above effective Lagragians, we obtain the following decay amplitudes for $\Lambda_b \to P_\psi^{1/2}K$ of Fig. 1

$$\begin{aligned}\mathcal{M}_1^a = i^3\int\frac{d^4q}{(2\pi)^4}&\left[g_{P_\psi^{1/2}\Lambda_c\bar{D}^*}\bar{u}(p_2)\gamma^\nu\gamma_5\left(g_{\mu\nu}-\frac{p_{2\mu}p_{2\nu}}{m^2_{P_\psi^{1/2}}}\right)(\not{q}_2+m_2)i(A+B\gamma_5)u(k_0)\right]\\ &\times[-g_{KD^*D_s}(q_1+p_1)_\alpha]\left(-g^{\mu\alpha}+\frac{q^\mu q^\alpha}{m_E^2}\right)\frac{1}{q_1^2-m_1^2}\frac{1}{q_2^2-m_2^2}\frac{1}{q^2-m_E^2},\end{aligned}$$

$$\mathcal{M}_1^b = i^3 \int \frac{d^4q}{(2\pi)^4} \left[g_{P_\psi^{1/2}\Lambda_c \bar{D}^*} \bar{u}(p_2)\gamma^\nu\gamma_5 \left(g_{\mu\nu} - \frac{p_{2\mu}p_{2\nu}}{m^2_{P_\psi^{1/2}}} \right) \right] (\not{q}_2 + m_2)$$
$$\times \left[\left(A_1\gamma_\alpha\gamma_5 + A_2\frac{q_{2\alpha}}{m}\gamma_5 + B_1\gamma_\alpha + B_2\frac{q_{2\alpha}}{m} \right) u(k_0) \right] [-g_{KD^*D_s^*}\varepsilon_{\rho\lambda\eta\tau}q^\rho q_1^\eta]$$
$$\times \left(-g^{\mu\lambda} + \frac{q^\mu q^\lambda}{m_E^2} \right) \left(-g^{\alpha\tau} + \frac{q_1^\alpha q_1^\tau}{m_1^2} \right) \frac{1}{q_1^2 - m_1^2} \frac{1}{q_2^2 - m_2^2} \frac{1}{q^2 - m_E^2},$$
$$\mathcal{M}_1^c = i^3 \int \frac{d^4q}{(2\pi)^4} \left[g_{P_\psi^{1/2}\Lambda_c \bar{D}} \bar{u}(p_2)(\not{q}_2 + m_2) \left(A_1\gamma_\alpha\gamma_5 + A_2\frac{q_{2\alpha}}{m}\gamma_5 + B_1\gamma_\alpha + B_2\frac{q_{2\alpha}}{m} \right) u(k_0) \right]$$
$$\times [-g_{KDD_s^*}(-q + p_1)_\tau] \left(-g^{\alpha\tau} + \frac{q_1^\alpha q_1^\tau}{m_1^2} \right) \frac{1}{q_1^2 - m_1^2} \frac{1}{q_2^2 - m_2^2} \frac{1}{q^2 - m_E^2}, \tag{18}$$

where k_0, q_1, q_2, q, p_1, and p_2 refer to the momenta of Λ_b, $D_s^{(*)}$, Λ_c, $\bar{D}^{(*)}$, K, and $P_\psi^{1/2}$, respectively, and $\bar{u}(p_2)$ and $u(k_0)$ represent the spinors of $P_\psi^{1/2}$ and Λ_b. Similarly, we write the decay amplitudes for $\Lambda_b \to P_\psi^{3/2}K$ of Fig. 2 as follows

$$\mathcal{M}_3^a = i^3 \int \frac{d^4q}{(2\pi)^4} [g_{P_\psi^{3/2}\Lambda_c \bar{D}^*} \bar{u}_\mu(p_2)](\not{q}_2 + m_2)[i(A + B\gamma_5)u(k_0)]$$
$$\times [-g_{KD^*D_s}(q_1 + p_1)_\nu] \left(-g^{\mu\nu} + \frac{q^\mu q^\nu}{m_E^2} \right) \frac{1}{q_1^2 - m_1^2} \frac{1}{q_2^2 - m_2^2} \frac{1}{q^2 - m_E^2},$$
$$\mathcal{M}_3^b = i^3 \int \frac{d^4q}{(2\pi)^4} \left[g_{P_\psi^{3/2}\Lambda_c \bar{D}^*} \bar{u}_\mu(p_2)(\not{q}_2 + m_2)(-i) \left(A_1\gamma_\alpha\gamma_5 + A_2\frac{q_{2\alpha}}{m}\gamma_5 + B_1\gamma_\alpha + B_2\frac{q_{2\alpha}}{m} \right) u(k_0) \right]$$
$$\times [-g_{KD^*D_s^*}\varepsilon_{\rho\lambda\eta\tau}q^\rho q_1^\eta] \left(-g^{\mu\lambda} + \frac{q^\mu q^\lambda}{m_E^2} \right) \left(-g^{\alpha\tau} + \frac{q_1^\alpha q_1^\tau}{m_1^2} \right) \frac{1}{q_1^2 - m_1^2} \frac{1}{q_2^2 - m_2^2} \frac{1}{q^2 - m_E^2}. \tag{19}$$

With the amplitudes for the decays of $\Lambda_b \to P_\psi^{1/2}K$ and $\Lambda_b \to P_\psi^{3/2}K$ given above, one can compute the corresponding partial decay widths

$$\Gamma = \frac{1}{2J+1} \frac{1}{8\pi} \frac{|\vec{p}|}{m_{\Lambda_b}^2} |\bar{M}|^2 \tag{20}$$

where J is the total angular momentum of the initial Λ_b baryon and $|\vec{p}|$ is the momentum of either final state in the rest frame of the Λ_b baryon.

Regarding the three-body decays of the pentaquark molecules, we have systematically investigated two decay modes: tree diagrams and triangle diagrams, and found that the former can almost saturate their total three-body decay widths [35]. In this work, with the new couplings between the pentaquark molecules and $\bar{D}^{(*)}\Sigma_c^{(*)}$, we update the widths of the three-body decays $P_\psi^N \to \bar{D}^{(*)}\Lambda_c\pi$, where these hidden-charm pentaquark molecules decay into $\bar{D}^{(*)}\Lambda_c\pi$ via the off-shell $\Sigma_c^{(*)}$ baryons decaying into $\Lambda_c\pi$. The details for the calculations can be found in our previous work [35].

III. RESULTS AND DISCUSSIONS

Because the three-body partial decay widths of the pentaquark states $P_\psi^N(4312)$, $P_\psi^N(4440)$, and $P_\psi^N(4457)$ as hadronic molecules are less than 1 MeV, we can neglect their three-body decays and assume that their two-body decays saturate their total widths. Therefore, we suppose that these three pentaquark molecules are dynamically generated via the $\bar{D}^{(*)}\Sigma_c^{(*)}$, $\bar{D}^{(*)}\Lambda_c$, $\eta_c N$, and $J/\psi N$ coupled-channel potentials. In the heavy quark limit, the contact potentials of this coupled-channel system are parametrized by seven parameters as shown in Eqs. (A6) and (A7). In this work, we set the potential $V_{J/\psi(\eta_c)N \to J/\psi(\eta_c)N} = 0$, resulting in six unknown parameters. The unknown couplings of the $\bar{D}^{(*)}\Sigma_c^{(*)} \to \bar{D}^{(*)}\Sigma_c^{(*)}$ potentials are well described by the light meson saturation approach [13], which is widely applied to study heavy hadronic molecules [18,95–97]. Therefore, we expect that the light meson saturation approach (see the Appendix B) is also valid for the $\bar{D}^{(*)}\Lambda_c \to \bar{D}^{(*)}\Lambda_c$ interaction. With the $\bar{D}^{(*)}\Sigma_c^{(*)} \to \bar{D}^{(*)}\Sigma_c^{(*)}$ potentials determined in Ref. [63], we obtain the $\bar{D}^{(*)}\Lambda_c \to \bar{D}^{(*)}\Lambda_c$ potentials using the light meson saturation approach, and then search for poles near the $\bar{D}^{(*)}\Lambda_c$ threshold, but find none, indicating that there exists no genuine states generated by the $\bar{D}^{(*)}\Lambda_c$ interactions, consistent with Refs. [9,12,98]. Very recently, Duan *et al.* argued that there exist the enhancements at the $\bar{D}^{(*)}\Lambda_c$ thresholds induced by the triangle and box singularities [99]. Therefore, even taking into account the $\bar{D}^{(*)}\Lambda_c$, $\eta_c N$, and $J/\psi N$ channels, the number of hidden-charm pentaquark molecules does not change. These channels mainly affect the imaginary part of the pole positions, i.e., the widths of the pentaquark states.

TABLE II. Masses and quantum numbers of hadrons relevant to this work [75].

Hadron	$I(J^P)$	M (MeV)	Hadron	$I(J^P)$	M (MeV)
p	$\frac{1}{2}(1/2^+)$	938.27	n	$\frac{1}{2}(1/2^+)$	939.57
Σ_c^{++}	$1(1/2^+)$	2453.97	Σ_c^+	$1(1/2^+)$	2452.65
Σ_c^{*+++}	$1(3/2^+)$	2518.41	Σ_c^{*+}	$1(3/2^+)$	2517.4
Σ_c^0	$1(1/2^+)$	2453.75	Σ_c^{*0}	$1(3/2^+)$	2518.48
Λ_c^+	$0(1/2^+)$	2286.46	Λ_b	$0(1/2^+)$	5619.60
$\pi^\pm$	$1(0^-)$	139.57	π^0	$1(0^-)$	134.98
$K^\pm$	$1/2(0^-)$	493.677	K^0	$1/2(0^-)$	497.611
$\bar{D}^0$	$\frac{1}{2}(0^-)$	1864.84	D^-	$\frac{1}{2}(0^-)$	1869.66
$\bar{D}^{*0}$	$\frac{1}{2}(1^-)$	2006.85	D^{*-}	$\frac{1}{2}(1^-)$	2010.26
$D_s^\pm$	$0(0^-)$	1968.35	$D_s^{*\pm}$	$0(1^-)$	2112.2
J/ψ	$0(1^-)$	3096.90	η_c	$0(0^-)$	2983.90

A. Widths of hidden-charm pentaquark molecules

In Table II, we tabulate the masses and quantum numbers of relevant particles. For the cutoff in the Gaussian regulator, we choose the value of $\Lambda = 1.5$ GeV [35]. To quantify the agreement with the experimental data, we use the χ^2 defined as

$$\chi^2 = \sum_{i=1}^{3} \frac{(M^i_{\rm exp} - M^i_{\rm fit})^2}{{d^i_M}^2} + \sum_{i=1}^{3} \frac{(\Gamma^i_{\rm exp} - \Gamma^i_{\rm fit})^2}{{d^i_\Gamma}^2} \quad (21)$$

where $M^i_{\rm exp}(\Gamma^i_{\rm exp})$ and $M^i_{\rm fit}(\Gamma^i_{\rm fit})$ are the masses(widths) measured by the LHCb Collaboration and those obtained in the contact-range EFT approach, d^i_M and d^i_Γ are the uncertainties of experimental masses and widths, and the superscripts with $i = 1$, $i = 2$, and $i = 3$ represent $P^N_\psi(4312)$, $P^N_\psi(4440)$, and $P^N_\psi(4457)$, respectively. The masses and decay widths of the three states are [2]

$$\begin{aligned}
M_{P^N_\psi(4312)} &= 4311.9 \pm 0.7^{+6.8}_{-0.6}\ \text{MeV},\\
\Gamma_{P^N_\psi(4312)} &= 9.8 \pm 2.7^{+3.7}_{-4.5}\ \text{MeV},\\
M_{P^N_\psi(4440)} &= 4440.3 \pm 1.3^{+4.1}_{-4.7}\ \text{MeV},\\
\Gamma_{P^N_\psi(4440)} &= 20.6 \pm 4.9^{+8.7}_{-10.1}\ \text{MeV},\\
M_{P^N_\psi(4457)} &= 4457.3 \pm 0.6^{+4.1}_{-1.7}\ \text{MeV},\\
\Gamma_{P^N_\psi(4457)} &= 6.4 \pm 2.0^{+5.7}_{-1.9}\ \text{MeV}.
\end{aligned} \quad (22)$$

TABLE III. Parameters C_a, C_b, C'_a, C'_b, g_1, and g_2 (in units of GeV^{-1}) determined by fitting to the masses and widths of $P^N_\psi(4312)$, $P^N_\psi(4440)$, and $P^N_\psi(4457)$ and the corresponding χ^2 in scenario A and scenario B.

Scenario	C_a	C_b	C'_a	C'_b	g_1	g_2	χ^2
A	−52.533	6.265	−11.366	2.669	20.360	−19.590	1.155
B	−56.030	−5.418	−12.120	−5.136	58.963	28.587	2.980

TABLE IV. Two-body decay widths, three-body decay widths, and total decay widths (in units of MeV) of hidden-charm pentaquark molecules in scenario A and scenario B.

Scenario	A					
Molecule	$P^N_{\psi 1}$	$P^N_{\psi 2}$	$P^N_{\psi 3}$	$P^N_{\psi 4}$	$P^N_{\psi 5}$	$P^N_{\psi 6}$
Two-body decay	7.00	5.40	17.20	1.40	19.80	15.40
Three-body decay	0.20	1.47	0.03	0.33	3.83	6.85
Total decay	7.20	6.87	17.23	1.73	23.63	22.25
Scenario	B					
Molecule	$P^N_{\psi 1}$	$P^N_{\psi 2}$	$P^N_{\psi 3}$	$P^N_{\psi 4}$	$P^N_{\psi 5}$	$P^N_{\psi 6}$
Two-body decay	8.00	12.40	2.20	9.00	15.00	7.40
Three-body decay	0.16	1.00	0.01	2.44	13.58	9.58
Total decay	8.16	13.40	2.21	11.44	28.58	16.98

Given the fact that the light meson saturation is valid for the $\bar{D}^{(*)}\Lambda_c \to \bar{D}^{(*)}\Lambda_c$ and $\bar{D}^{(*)}\Sigma_c^{(*)} \to \bar{D}^{(*)}\Sigma_c^{(*)}$ potentials,[2] we adopt the ratio $C'_a/C_a = 0.216$ obtained in the light meson saturation approach. As a result, there only remain five parameters. With the above preparations we determine the values of the parameters C_a, C_b, C'_b, g_1, and g_2 as well as the χ^2 for scenario A and scenario B and show them in Table III. In the following, we compare the fitted parameters (C_a, C_b, and C'_b) with those obtained in the light meson saturation approach (see the Appendix B for details). With the light meson saturation, we obtain the ratio $C_b/C_a = 0.12$, while the ratio determined in the EFT approach (by fitting to the data) is $C_b/C_a = -0.12$ and $C_b/C_a = 0.10$ for scenario A and scenario B, respectively. It seems that the light meson saturation approach prefers scenario B, consistent with the single-channel analysis [13]. Moreover, the light meson saturation approach yields $C'_b/C_b = 0.61$, while the value determined in the EFT approach is $C'_b/C_b = 0.43$ for scenario A but $C'_b/C_b = 0.95$ for scenario B. One can see that they are quite different for either scenario A or scenario B. From the perspective of light meson saturation, only the ρ meson exchange is considered to saturate the $\bar{D}^{(*)}\Sigma_c \to \bar{D}^{(*)}\Lambda_c$ interactions. However, the one-pion exchange plays a significant role in the $\bar{D}^{(*)}\Sigma_c \to \bar{D}^{(*)}\Lambda_c$ potentials [11,12,37]. Since the one-pion exchange is not considered, the C'_b obtained in the light meson saturation approach is not consistent with the C'_b determined in the EFT approach for either scenario A or scenario B.

In Table V, we present the pole positions of the hidden-charm pentaquark molecules and the couplings to their constituents. From the obtained pole positions of $P^N_\psi(4312)$, $P^N_\psi(4440)$, and $P^N_\psi(4457)$, it is obvious that scenario A,

[2]As indicated in Ref. [13], the ratio of C_a to C_b estimated by the light meson saturation approach is consistent with that obtained by the contact-range EFT approach.

TABLE V. Pole positions (in units of MeV) of six hidden-charm pentaquark molecules and the couplings to their constituents in scenario A and scenario B.

Scenario	A					
Name	$P_{\psi 1}^N$	$P_{\psi 2}^N$	$P_{\psi 3}^N$	$P_{\psi 4}^N$	$P_{\psi 5}^N$	$P_{\psi 6}^N$
Molecule	$\bar{D}\Sigma_c$	$\bar{D}\Sigma_c^*$	$\bar{D}^*\Sigma_c$	$\bar{D}^*\Sigma_c$	$\bar{D}^*\Sigma_c^*$	$\bar{D}^*\Sigma_c^*$
J^P	$\frac{1}{2}^-$	$\frac{3}{2}^-$	$\frac{1}{2}^-$	$\frac{3}{2}^-$	$\frac{1}{2}^-$	$\frac{3}{2}^-$
Pole (MeV)	$4310.6+3.5i$	$4372.8+2.7i$	$4440.6+8.6i$	$4458.4+0.7i$	$4500.0+9.9i$	$4513.2+7.7i$
$g_{P_\psi^N\Sigma_c^*\bar{D}^*}$	⋯	⋯	⋯	⋯	2.686	2.194
$g_{P_\psi^N\Sigma_c\bar{D}^*}$	⋯	⋯	2.554	1.082	0.141	0.218
$g_{P_\psi^N\Sigma_c^*\bar{D}}$	⋯	2.133	⋯	0.179	⋯	0.237
$g_{P_\psi^N\Sigma_c\bar{D}}$	2.089	⋯	0.254	⋯	0.139	⋯
$g_{P_\psi^N\Lambda_c\bar{D}^*}$	0.234	0.074	0.177	0.050	0.110	0.241
$g_{P_\psi^N\Lambda_c\bar{D}}$	0.014	⋯	0.158	⋯	0.207	⋯
$g_{P_\psi^N J/\psi N}$	0.251	0.454	0.584	0.103	0.434	0.532
$g_{P_\psi^N\eta_c N}$	0.420	⋯	0.261	⋯	0.527	⋯
Scenario	B					
Name	$P_{\psi 1}^N$	$P_{\psi 2}^N$	$P_{\psi 3}^N$	$P_{\psi 4}^N$	$P_{\psi 5}^N$	$P_{\psi 6}^N$
Molecule	$\bar{D}\Sigma_c$	$\bar{D}\Sigma_c^*$	$\bar{D}^*\Sigma_c$	$\bar{D}^*\Sigma_c$	$\bar{D}^*\Sigma_c^*$	$\bar{D}^*\Sigma_c^*$
J^P	$\frac{1}{2}^-$	$\frac{3}{2}^-$	$\frac{1}{2}^-$	$\frac{3}{2}^-$	$\frac{1}{2}^-$	$\frac{3}{2}^-$
Pole (MeV)	$4309.9+4i$	$4365.8+6.2i$	$4458.4+4.5i$	$4441.4+1.1i$	$4521.6+7.5i$	$4522.5+3.7i$
$g_{P_\psi^N\Sigma_c^*\bar{D}^*}$	⋯	⋯	⋯	⋯	1.841	1.621
$g_{P_\psi^N\Sigma_c\bar{D}^*}$	⋯	⋯	1.679	2.462	0.107	0.143
$g_{P_\psi^N\Sigma_c^*\bar{D}}$	⋯	2.451	⋯	0.099	⋯	0.171
$g_{P_\psi^N\Sigma_c\bar{D}}$	2.072	⋯	0.161	⋯	0.131	⋯
$g_{P_\psi^N\Lambda_c\bar{D}^*}$	0.392	0.090	0.247	0.159	0.232	0.223
$g_{P_\psi^N\Lambda_c\bar{D}}$	0.020	⋯	0.191	⋯	0.281	⋯
$g_{P_\psi^N J/\psi N}$	0.263	0.704	0.277	0.168	0.314	0.312
$g_{P_\psi^N\eta_c N}$	0.413	⋯	0.164	⋯	0.328	⋯

yielding results consistent with the experimental data, is better than scenario B, which is quite different from the single-channel study [63]. Our study shows that the coupled-channel effects can help distinguish the two possible scenarios. In a similar approach but without the $\bar{D}^{(*)}\Lambda_c$ channels, scenario A is still slightly better than scenario B [35]. We note in passing that the chiral unitary model [9] also prefers scenario A. We further note that the coefficients in the contact-range potentials of Eqs. (A6) and (A7) are derived assuming the HQSS, while the HQSS breaking is not taken into account. In Ref. [11], it was shown that the tensor term of the one-pion exchange potentials plays a crucial role in describing the widths of the pentaquark molecules, while the D-wave potentials are neglected in this work. Therefore, we cannot conclude which scenario is more favorable at this stage.

Up to now, the spins of $P_\psi^N(4440)$ and $P_\psi^N(4457)$ are still undetermined experimentally, which motivated many theoretical discussions on how to determine their spins [21,23,100]. One crucial issue is that the strength of $\bar{D}^*\Sigma_c \to \bar{D}^*\Sigma_c$ potentials of $J^P = 1/2^-$ and $J^P = 3/2^-$ are undetermined. We can see that the $J^P = 1/2^-$ $\bar{D}^*\Sigma_c \to \bar{D}^*\Sigma_c$ potential is stronger than the $J^P = 3/2^-$ $\bar{D}^*\Sigma_c \to \bar{D}^*\Sigma_c$ potential in scenario A, while their order reverses in scenario B. In Refs. [34,37], Burns *et al.* proposed another case, named as scenario C, which actually corresponds to a special case of scenario B, where the $J^P = 1/2^-$ $\bar{D}^*\Sigma_c \to \bar{D}^*\Sigma_c$ potential is not strong enough to form a bound state, and therefore $P_\psi^N(4457)$ is interpreted as a kinetic effect rather than a genuine state. From their values of C_a and C_b [34], the ratio C_b/C_a is determined to be around 0.5, which implies the emergence of a large spin-spin interaction, inconsistent with the principle of EFTs. It is no surprise that such a large spin-spin interaction breaks the completeness of the multiplet picture of hidden-charm pentaquark molecules [9,11,12,16,18,21,63–66]. Therefore, we strongly recommend that lattice QCD simulations could study the potentials of $J^P = 1/2^-$ $\bar{D}^*\Sigma_c$ and $J^P = 3/2^-$ $\bar{D}^*\Sigma_c$ to address this issue.[3]

[3]A recent lattice QCD study shows that there exists a $J^P = 1/2^-\bar{D}^*\Sigma_c$ bound state with a binding energy of 6 MeV [101].

The imaginary parts of the pole positions in Table V specify the two-body partial decay widths of the pentaquark molecules, which can also be calculated via the triangle diagrams using the effective Lagrangian approach [65,102]. From the results of Table V, we can calculate the two-body decay widths of these pentaquark molecules and tabulate them in Table IV. Moreover, with the newly obtained couplings $g_{P_\psi^N\bar{D}^{(*)}\Sigma_c^{(*)}}$, we update their three-body decay widths as shown in Table IV. Comparing with the results in Ref. [35], we find that the new results vary a bit because the pole positions affect the phase space of the three-body decays and the values of the couplings $g_{P_\psi^N\bar{D}^{(*)}\Sigma_c^{(*)}}$. Assuming that the two-body and three-body decays are dominant decay channels for the pentaquark molecules, we can obtain their total decay widths by summing the two decay modes. Our results indicate that the widths of $P_{\psi 5}^N$ and $P_{\psi 6}^N$ as the $\bar{D}^*\Sigma_c^*$ molecules are larger than those of $P_\psi^N(4312)$, $P_\psi^N(4440)$, and $P_\psi^N(4457)$ reported by the LHCb Collaboration, and their three-body decay widths account for a large proportion of their total widths. In addition, we can see that the three-body decay widths of $P_\psi^N(4312)$, $P_\psi^N(4440)$, and $P_\psi^N(4457)$ account for only a small proportion of their total widths, which confirms our assumption that their total widths are almost saturated by the two-body decays.

B. Production rates of hidden-charm pentaquark molecules

From the values of the couplings given in Table V, one can see that the $\bar{D}^{(*)}\Sigma_c^{(*)}$ channel plays a dominant role in generating these pentaquark molecules. Yet their productions in the Λ_b decay cannot proceed via the $\bar{D}^{(*)}\Sigma_c^{(*)}$ interactions as discussed above. It is important to investigate the productions of hidden-charm pentaquark molecules in the Λ_b decays via the $\bar{D}^{(*)}\Lambda_c$ interactions although the couplings of the pentaquark states to $\bar{D}^{(*)}\Lambda_c$ are small. With the couplings $g_{P_\psi^N\bar{D}^{(*)}\Lambda_c}$ given in Table V, we employ the effective Lagrangian approach to calculate the decays of $\Lambda_b \to P_\psi^N K$ illustrated in Figs. 1 and 2.

In Table VI, we present the branching fractions of $\Lambda_b \to P_\psi^N K$ in scenario A and scenario B. Our results show that the branching factions of the three pentaquark states discovered by the LHCb Collaboration: $\mathcal{B}(\Lambda_b \to P_\psi^N(4312)K) = 35.18 \times 10^{-6}$, $\mathcal{B}(\Lambda_b \to P_\psi^N(4440)K) = 15.30 \times 10^{-6}$, and $\mathcal{B}(\Lambda_b \to P_\psi^N(4457)K) = 0.48 \times 10^{-6}$ in scenario A and $\mathcal{B}(\Lambda_b \to P_\psi^N(4312)K) = 98.88 \times 10^{-6}$, $\mathcal{B}(\Lambda_b \to P_\psi^N(4440)K) = 5.21 \times 10^{-6}$, and $\mathcal{B}(\Lambda_b \to P_\psi^N(4457)K) = 27.23 \times 10^{-6}$ in scenario B. From the order of magnitude of the obtained branching fractions, we can conclude that the pentaquark molecules can be produced via the triangle diagrams shown in Figs. 1 and 2. The branching fractions of the decay $\Lambda_b \to P_\psi^N(4312)K$ are larger than those of $\Lambda_b \to P_\psi^N(4440)K$ and $\Lambda_b \to P_\psi^N(4457)K$ in both cases, and the branching fractions involving $P_\psi^N(4440)$ and $P_\psi^N(4457)$ for $J^P = 1/2^-$ are always larger than those for $J^P = 3/2^-$. Such results reflect that the branching fractions of the decays $\Lambda_b \to P_\psi^N K$ are related to the couplings $g_{P_\psi^N\bar{D}^{(*)}\Lambda_c}$, especially the coupling $g_{P_\psi^N\bar{D}^*\Lambda_c}$, which shows that the $\bar{D}^*\Lambda_c$ interactions play an important role in producing the pentaquark molecules in the Λ_b decays. Similarly, we predict the branching fractions of Λ_b decaying into $P_{\psi 2}^N$, $P_{\psi 5}^N$, and $P_{\psi 6}^N$ plus a kaon as shown in Table VI, the order of magnitude of which are similar to those involving $P_\psi^N(4440)$ and $P_\psi^N(4457)$.

TABLE VI. Branching fractions (10^{-6}) of Λ_b decaying into a K meson and a hidden-charm pentaquark molecule in scenario A and scenario B.

Scenario	A					
Molecule	$P_{\psi 1}^N$	$P_{\psi 2}^N$	$P_{\psi 3}^N$	$P_{\psi 4}^N$	$P_{\psi 5}^N$	$P_{\psi 6}^N$
$\mathcal{B}(\Lambda_b \to P_\psi^N K)$	35.18	1.49	15.30	0.48	6.37	9.01
Scenario	B					
Molecule	$P_{\psi 1}^N$	$P_{\psi 2}^N$	$P_{\psi 3}^N$	$P_{\psi 4}^N$	$P_{\psi 5}^N$	$P_{\psi 6}^N$
$\mathcal{B}(\Lambda_b \to P_\psi^N K)$	98.88	2.27	27.23	5.21	21.69	7.43

Up to now, there exist no available experimental data for the branching fractions of the decays $\Lambda_b \to P_\psi^N K$. The LHCb Collaboration measured the relevant ratios of branching fractions for the three pentaquark states: $R_{P_\psi^N(4312)} = (0.30 \pm 0.07^{+0.34}_{-0.09})\%$, $R_{P_\psi^N(4440)} = (1.11 \pm 0.33^{+0.22}_{-0.11})\%$, and $R_{P_\psi^N(4457)} = (0.53 \pm 0.16^{+0.15}_{-0.13})\%$, where R is defined as

$$R_{P_\psi^{N+}} = \frac{\mathcal{B}(\Lambda_b^0 \to P_\psi^{N+}K^-) \cdot \mathcal{B}(P_\psi^{N+} \to J/\psi p)}{\mathcal{B}(\Lambda_b^0 \to J/\psi p K^-)} \tag{23}$$

According to RPP [75], the branching fraction of $\Lambda_b^0 \to J/\psi p K^-$ is $\mathcal{B}(\Lambda_b^0 \to J/\psi p K^-) = 3.2^{+0.6}_{-0.5} \times 10^{-4}$, and then we obtain the product of the branching fractions of the decays $\Lambda_b \to P_\psi^N K$ and $P_\psi^N \to J/\psi p$

$$\begin{aligned}
&\mathcal{B}(\Lambda_b^0 \to P_\psi^N(4312)^+K^-) \cdot \mathcal{B}(P_\psi^N(4312)^+ \to J/\psi p) = 0.96^{+1.13}_{-0.39} \times 10^{-6},\\
&\mathcal{B}(\Lambda_b^0 \to P_\psi^N(4440)^+K^-) \cdot \mathcal{B}(P_\psi^N(4440)^+ \to J/\psi p) = 3.55^{+1.43}_{-1.24} \times 10^{-6},\\
&\mathcal{B}(\Lambda_b^0 \to P_\psi^N(4457)^+K^-) \cdot \mathcal{B}(P_\psi^N(4457)^+ \to J/\psi p) = 1.70^{+0.77}_{-0.71} \times 10^{-6}.
\end{aligned} \tag{24}$$

TABLE VII. Two-body partial decay widths (in units of MeV) of hidden-charm pentaquark molecules as well as their branching fractions in scenario A and scenario B.

Scenario	A					
Molecule	$P^N_{\psi 1}$	$P^N_{\psi 2}$	$P^N_{\psi 3}$	$P^N_{\psi 4}$	$P^N_{\psi 5}$	$P^N_{\psi 6}$
$\Gamma_2(\Sigma_c\bar{D}^*)$	⋯	⋯	⋯	⋯	0.50 (2.52%)	1.38 (8.87%)
$\Gamma_3(\Sigma_c^*\bar{D})$	⋯	⋯	⋯	1.14(73.23%)	⋯	2.62 (16.87%)
$\Gamma_4(\Sigma_c\bar{D})$	⋯	⋯	2.87 (16.59%)	⋯	1.04 (5.29%)	⋯
$\Gamma_5(\Lambda_c\bar{D}^*)$	0.83 (11.71%)	0.19 (3.48%)	1.44 (8.33%)	0.12 (7.82%)	0.65 (3.32%)	3.24 (20.81%)
$\Gamma_6(\Lambda_c\bar{D})$	0.01 (0.14%)	⋯	1.60 (9.22%)	⋯	2.98 (15.14%)	⋯
$\Gamma_7(J/\psi N)$	1.43 (20.22%)	5.16 (96.52%)	9.29 (53.64%)	0.29 (18.95%)	5.46 (27.73%)	8.31 (53.45%)
$\Gamma_8(\eta_c N)$	4.81 (67.93%)	⋯	2.12 (12.23%)	⋯	9.06 (45.98%)	⋯
Scenario	B					
Molecule	$P^N_{\psi 1}$	$P^N_{\psi 2}$	$P^N_{\psi 3}$	$P^N_{\psi 4}$	$P^N_{\psi 5}$	$P^N_{\psi 6}$
$\Gamma_2(\Sigma_c\bar{D}^*)$	⋯	⋯	⋯	⋯	0.36 (2.17%)	0.64 (8.30%)
$\Gamma_3(\Sigma_c^*\bar{D})$	⋯	⋯	⋯	0.31 (13.63%)	⋯	1.41 (18.19%)
$\Gamma_4(\Sigma_c\bar{D})$	⋯	⋯	1.23 (12.88%)	⋯	0.98 (5.92%)	⋯
$\Gamma_5(\Lambda_c\bar{D}^*)$	2.27 (26.71%)	0.26 (2.10%)	2.97 (30.92%)	1.17 (52.05%)	3.05 (18.48%)	2.82 (36.37%)
$\Gamma_6(\Lambda_c\bar{D})$	0.02 (0.23%)	⋯	2.40 (25.03%)	⋯	5.65 (34.18%)	⋯
$\Gamma_7(J/\psi N)$	1.57 (18.45%)	12.28 (97.90%)	2.13 (22.26%)	0.77 (34.33%)	2.92 (17.67%)	2.88 (37.14%)
$\Gamma_8(\eta_c N)$	4.65 (54.61%)	⋯	0.85 (8.86%)	⋯	3.57 (21.58%)	⋯

To compare with the experimental data, we have to obtain the branching fractions of P^N_ψ decaying into $J/\psi p$, which are not yet determined experimentally. We note that the GlueX and JLab Collaborations investigated the production rates of pentaquark states in the photoproduction process and only gave the upper limits of $\mathcal{B}(P^N_\psi \to J/\psi p) < 2.0\%$ [38,39], which indicates that the branching fractions of $\mathcal{B}(\Lambda_b^0 \to P^{N+}_\psi K^-)$ are at the order of 10^{-4}, approaching to the values of $\mathcal{B}(\Lambda_b^0 \to J/\psi p K^-)$. Such large values highlight the inconsistency between the LHCb results and the GlueX/JLab results. Therefore, more precise experimental data are needed to settle this issue.

Using Eq. (17), we calculate the two-body partial decay widths of hidden-charm pentaquark molecules, and then estimate the branching fractions of the decays $P^N_\psi \to J/\psi p$. The results are shown in Table VII, where the three-body decay widths of the pentaquark molecules are not included. One can see that the partial decay widths of $P^N_\psi \to \bar{D}^{(*)}\Lambda_c$ are less than those of $P^N_\psi \to J/\psi p$ in scenario A, but their order reverses in scenario B. In Ref. [103], the estimated branching fractions of the decays $P^N_\psi \to \bar{D}^{(*)}\Lambda_c$ are much smaller than those of the decays $P^N_\psi \to J/\psi p$, consistent with scenario A. In terms of the meson exchange theory, the branching fractions of the decays $P^N_\psi \to \bar{D}^{(*)}\Lambda_c$ are larger than those of the decays $P^N_\psi \to J/\psi p$, where the heavy meson $[\bar{D}^{(*)}]$ exchange and the light meson $[\pi(\rho)]$ exchange are responsible for the $\bar{D}^{(*)}\Sigma_c^{(*)} \to J/\psi p$ and $\bar{D}^{(*)}\Sigma_c^{(*)} \to \bar{D}^{(*)}\Lambda_c$ interactions, respectively [65]. It is obvious that the transitions $\bar{D}^{(*)}\Sigma_c^{(*)} \to J/\psi p$ are heavily suppressed, resulting in the small partial decay widths of $P^N_\psi \to J/\psi p$ in the same theoretical framework [65]. We note that the meson exchange theory has been tested for light mesons exchanges, but remains to be verified for heavy meson exchanges, especially when both heavy and light mesons can be exchanged. The meson exchange theory dictates that charmed mesons are responsible for the very short range interaction, but they cannot adequately describe such short-range interactions because one gluon exchange may play a role. In Ref. [104], the authors found that the strength of the short range potential provided by the one gluon exchange is much stronger than that provided by the heavy meson exchange. In the present work, the hidden-charm meson-baryon potentials are provided by the contact-range EFT constrained by HQSS with the low-energy constants determined by fitting to data, which are plausible but the underlying mechanism needs to be clarified.

With the obtained branching fractions $\mathcal{B}(\Lambda_b \to P^N_\psi K)$ in Table VI and $\mathcal{B}(P^N_\psi \to J/\psi p)$ in Table VII, we further calculate the branching fractions $\mathcal{B}[\Lambda_b \to (P^N_\psi \to J/\psi p)K]$ for scenario A and scenario B as shown Table VIII. Our results show that the branching fractions for $P^N_\psi(4312)$ and $P^N_\psi(4440)$ are of the same order as their experimental counterparts, but the branching fraction for $P^N_\psi(4457)$ is smaller by one order of magnitude. For scenario B, the branching fractions for $P^N_\psi(4440)$ and $P^N_\psi(4457)$ are of the same order as their experimental counterparts, but the branching fraction for $P^N_\psi(4312)$ is larger by one order of magnitude. We can see that our model cannot simultaneously describe the branching fractions of these three

TABLE VIII. Branching fractions (10^{-6}) of the decays $\Lambda_b \to (P_\psi^N \to J/\psi p)K$ in scenario A and scenario B.

Scenario	A					
Molecule	$P_{\psi 1}^N$	$P_{\psi 2}^N$	$P_{\psi 3}^N$	$P_{\psi 4}^N$	$P_{\psi 5}^N$	$P_{\psi 6}^N$
Ours	7.11	1.44	8.21	0.09	1.77	4.82
ChUA [103]	1.82	8.62	0.13	0.83	0.04	2.36
LHCb [2]	0.96	⋯	3.55	1.70	⋯	⋯
Scenario	B					
Molecule	$P_{\psi 1}^N$	$P_{\psi 2}^N$	$P_{\psi 3}^N$	$P_{\psi 4}^N$	$P_{\psi 5}^N$	$P_{\psi 6}^N$
Ours	18.24	2.22	6.06	1.79	3.83	2.76
ChUA [103]	⋯	⋯	⋯	⋯	⋯	⋯
LHCb [2]	0.96	⋯	1.70	3.55	⋯	⋯

pentaquark states. In Ref. [103], the ChUA estimated the couplings $g_{P_\psi^N \bar{D}^{(*)}\Lambda_c}$ and the branching fractions $\mathcal{B}(P_\psi^N \to J/\psi p)$, which actually corresponds to scenario A of our results. Using the values estimated by ChUA we recalculate the branching fractions $\mathcal{B}[\Lambda_b \to (P_\psi^N \to J/\psi p)K]$ as shown in Table VIII. The branching fractions for $P_\psi^N(4312)$ and $P_\psi^N(4457)$ are of the same order as their experimental counterparts, but the branching fraction for $P_\psi^N(4440)$ is smaller by one order of magnitude. Obviously, the branching fractions for $P_\psi^N(4312)$, $P_\psi^N(4440)$, and $P_\psi^N(4457)$ in our model are related to the couplings of the pentaquark molecules to $\bar{D}^{(*)}\Lambda_c$ and $J/\psi p$. Nevertheless, the production mechanism of these three pentaquark states via the triangle diagrams shown in Figs. 1 and 2 is capable of qualitatively reproducing the experimental data, which further corroborates the hadronic molecular picture of these pentaquark states.

In Table VIII, we show the branching fractions for the HQSS partners of $P_\psi^N(4312)$, $P_\psi^N(4440)$, and $P_\psi^N(4457)$, where only the two-body decay modes contribute to the branching fractions of the decays $P_\psi^N \to J/\psi p$. As shown in Table IV, the three-body decay widths of $P_{\psi 2}^N$, $P_{\psi 5}^N$, and $P_{\psi 6}^N$ are up to several MeV. If taking into account the three-body decay widths, the branching fractions of $P_{\psi 2}^N$, $P_{\psi 5}^N$, and $P_{\psi 6}^N$ decaying into $J/\psi p$ become $\mathcal{B}(P_{\psi 2}^N \to J/\psi p) = 75\%$, $\mathcal{B}(P_{\psi 5}^N \to J/\psi p) = 23\%$, and $\mathcal{B}(P_{\psi 6}^N \to J/\psi p) = 37\%$ in scenario A and $\mathcal{B}(P_{\psi 2}^N \to J/\psi p) = 91\%$, $\mathcal{B}(P_{\psi 5}^N \to J/\psi p) = 10\%$, and $\mathcal{B}(P_{\psi 6}^N \to J/\psi p) = 17\%$ in scenario B. As result, the corresponding branching fractions of the decays $\Lambda_b \to (P_\psi^N \to J/\psi p)K$ reduce to $\mathcal{B}[\Lambda_b \to (P_{\psi 2}^N \to J/\psi p)K] = 1.11 \times 10^{-6}$, $\mathcal{B}[\Lambda_b \to (P_{\psi 5}^N \to J/\psi p)K] = 1.47 \times 10^{-6}$ and $\mathcal{B}[\Lambda_b \to (P_{\psi 6}^N \to J/\psi p)K] = 3.37 \times 10^{-6}$ in scenario A and $\mathcal{B}[\Lambda_b \to (P_{\psi 2}^N \to J/\psi p)K] = 2.08 \times 10^{-6}$, $\mathcal{B}[\Lambda_b \to (P_{\psi 5}^N \to J/\psi p)K] = 2.22 \times 10^{-6}$ and $\mathcal{B}[\Lambda_b \to (P_{\psi 6}^N \to J/\psi p)K] = 1.26 \times 10^{-6}$ in scenario B. We can see that the branching fractions of the pentaquark states $P_{\psi 2}^N$, $P_{\psi 5}^N$, and $P_{\psi 6}^N$ as hadronic molecules are smaller than those of $P_\psi^N(4312)$ and sum of $P_\psi^N(4440)$ and $P_\psi^N(4457)$ in scenario A and scenario B, which is consistent with the fact that these three HQSS partners have not been seen in the LHCb data sample of 2019.

TABLE IX. Branching fractions(10^{-6}) of the decays $\Lambda_b \to (P_\psi^N \to \bar{D}^*\Lambda_c)K$ in scenario A and scenario B.

Scenario	A					
Molecule	$P_{\psi 1}^N$	$P_{\psi 2}^N$	$P_{\psi 3}^N$	$P_{\psi 4}^N$	$P_{\psi 5}^N$	$P_{\psi 6}^N$
Ours	4.12	0.05	1.27	0.00	0.21	1.87
Scenario	B					
Molecule	$P_{\psi 1}^N$	$P_{\psi 2}^N$	$P_{\psi 3}^N$	$P_{\psi 4}^N$	$P_{\psi 5}^N$	$P_{\psi 6}^N$
Ours	26.41	0.05	8.42	2.71	4.01	2.70

These hidden-charm pentaquark molecules can be seen in the $J\psi p$ invariant mass distribution, and one can also expect to see them in the $\bar{D}^*\Lambda_c$ invariant mass distribution. Therefore, with the same approach we calculate the branching fractions of the decays $\Lambda_b \to (P_\psi^N \to \bar{D}^*\Lambda_c)K$ and the results are shown in Table IX. We can see that the branching fractions of the pentaquark molecules in the decays $\Lambda_b \to (P_\psi^N \to J/\psi p)K$ and $\Lambda_b \to (P_\psi^N \to \bar{D}^*\Lambda_c)K$ are similar except for $P_{\psi 2}^N$. The branching fraction $\mathcal{B}[\Lambda_b \to (P_{\psi 2}^N \to \bar{D}^*\Lambda_c)K]$ is smaller than the branching fraction $\mathcal{B}[\Lambda_b \to (P_{\psi 2}^N \to J/\psi p)K]$ by two order of magnitude. We encourage experimental searches for these pentaquark states in the $\bar{D}^*\Lambda_c$ invariant mass distributions of the Λ_b decays.

IV. SUMMARY AND OUTLOOK

The three pentaquark states $P_\psi^N(4312)$, $P_\psi^N(4440)$, and $P_\psi^N(4457)$ can be nicely arranged into a complete multiplet of $\bar{D}^{(*)}\Sigma_c^{(*)}$ hadronic molecules, while their partial decay widths and production rates in the Λ_b decay remain undetermined. In this work, we employed the contact-range effective field theory approach to dynamically generate the pentaquark molecules via the $\bar{D}^{(*)}\Sigma_c^{(*)}$, $\bar{D}^{(*)}\Lambda_c$, $J/\psi p$, and $\eta_c p$ coupled-channel interactions, where the six relevant unknown parameters were determined by fitting to the experimental data. With the obtained pole positions, we estimated the couplings of the pentaquark molecules to their constituents $J/\psi p$ and $\bar{D}^*\Lambda_c$, and then calculated the productions rates of these molecules in the Λ_b decays via the triangle diagrams, where the Λ_b baryon weakly decays into $\Lambda_c D_s^{(*)}$, then the $D_s^{(*)}$ mesons scatter into $\bar{D}^{(*)}K$, and finally the pentaquark molecules are dynamically generated by the $\bar{D}^*\Lambda_c$ interactions. In this work, with no extra

parameters (except those contained in the contact range EFT approach and determined by their masses and widths) we took the effective Lagrangian approach to calculate the triangle diagrams and their production rates in the Λ_b decays.

Our results showed that the masses of the three pentaquark states are well described either in scenario A or scenario B, which confirmed our previous conclusion that we cannot determine the favorable scenario in terms of their masses alone. However, we found that scenario A is more favored than scenario B once their widths are taken into account. Moreover, our results showed that their couplings to $\bar{D}^{(*)}\Lambda_c$ are smaller than those to $J/\psi p$ in scenario A, but larger in scenario B. For the branching fractions of the decays $\Lambda_b \to P_\psi^N K$, that of the $P_\psi^N(4312)$ is the largest and those of $P_\psi^N(4440)$ and $P_\psi^N(4457)$ with $J = 1/2$ are always larger than those with $J = 3/2$ in both scenario A and scenario B. Moreover, we predicted the following branching fractions: $\mathcal{B}[\Lambda_b \to P_{\psi 2}^N K] = (1\text{–}2) \times 10^{-6}$, $\mathcal{B}[\Lambda_b \to P_{\psi 5}^N K] = (6\text{–}22) \times 10^{-6}$, and $\mathcal{B}[\Lambda_b \to P_{\psi 6}^N K] = (7\text{–}9) \times 10^{-6}$, respectively.

With the couplings between the molecules and their constituents determined, we estimated the branching fractions $\mathcal{B}(P_\psi^N \to J/\psi p)$, and then obtained the branching fraction $\mathcal{B}[\Lambda_b \to (P_\psi^N \to J/\psi p)K]$. Our results showed that such branching fractions for $P_\psi^N(4312)$ and $P_\psi^N(4440)$ are consistent with the experimental data, while that for $P_\psi^N(4457)$ is larger than the experimental data in scenario A. For scenario B, the branching fractions for $P_\psi^N(4440)$ and $P_\psi^N(4457)$ are consistent with the experimental data, while that for $P_\psi^N(4312)$ is larger than the experimental data. Given the complicated nature of these decays and the various physical processes involved, we deem the agreements with the existing data acceptable. Therefore, we conclude that the three pentaquark states as hidden-charm meson-baryon molecules can be dynamically generated via the $\bar{D}^{(*)}\Lambda_c$ interactions in the Λ_b decay, which further corroborated the molecular interpretations of the pentaquark states. Moreover, the branching fractions of the HQSS partners of $P_\psi^N(4312)$, $P_\psi^N(4440)$, and $P_\psi^N(4457)$ are estimated to be the order of 10^{-6}, smaller than that of $P_\psi^N(4312)$ and the sum of those of $P_\psi^N(4440)$ and $P_\psi^N(4457)$. Therefore, we can attribute the nonobservation of the other HQSS partners in the decay $\Lambda_b \to (P_\psi^N \to J/\psi p)K$ to their small production rates. As a by-product, we further predicted the production rates of the pentaquark molecules in the decays $\Lambda_b \to (P_\psi^N \to \bar{D}^*\Lambda_c)K$.

ACKNOWLEDGMENTS

We are grateful to Eulogio Oset, Fu-Sheng Yu, Chu-Wen Xiao, Jun-Xu Lu, and Qi Wu for useful discussions. This work is supported in part by the National Natural Science Foundation of China under Grants No. 11975041 and No. 11961141004. M.-Z. L. acknowledges support from the National Natural Science Foundation of China under Grant No. 12105007.

APPENDIX A: CONTACT-RANGE POTENTIALS

To systematically generate the complete multiplet of hidden-charm pentaquark molecules, we take into account the $\bar{D}^{(*)}\Lambda_c$ channels in the $\bar{D}^{(*)}\Sigma_c^{(*)}$ coupled-channel systems, where the HQSS plays an important role. First, we express the spin wave function of the $\bar{D}^{(*)}\Sigma_c^{(*)}$ pairs in terms of the spins of the heavy quarks s_{1h} and s_{2h} and those of the light quark(s) (often referred to as brown mucks [105,106]) s_{1l} and s_{2l}, where 1 and 2 denote $\bar{D}^{(*)}$ and $\Sigma_c^{(*)}$, respectively, via the following spin coupling formula,

$$\begin{aligned}&|s_{1l}, s_{1h}, j_1; s_{2l}, s_{2h}, j_2; J\rangle \\ &= \sqrt{(2j_1+1)(2j_2+1)(2s_L+1)(2s_H+1)} \begin{pmatrix} s_{1l} & s_{2l} & s_L \\ s_{1h} & s_{2h} & s_H \\ j_1 & j_2 & J \end{pmatrix} \\ &\times |s_{1l}, s_{2l}, s_L; s_{1h}, s_{2h}, s_H; J\rangle. \end{aligned} \tag{A1}$$

The total light quark spin s_L and heavy quark spin s_H are given by $s_L = s_{1l} \otimes s_{2l}$ and $s_H = s_{1H} \otimes s_{2H}$, respectively.

More explicitly, for the $\bar{D}^{(*)}\Sigma_c$ states, the decompositions read

$$|\Sigma_c \bar{D}(1/2^-)\rangle = \frac{1}{2} 0_H \otimes 1/2_L + \frac{1}{2\sqrt{3}} 1_H \otimes 1/2_L + \sqrt{\frac{2}{3}} 1_H \otimes 3/2_L,$$

$$|\Sigma_c^* \bar{D}(3/2^-)\rangle = -\frac{1}{2} 0_H \otimes 3/2_L + \frac{1}{\sqrt{3}} 1_H \otimes 1/2_L + \frac{\sqrt{\frac{5}{3}}}{2} 1_H \otimes 3/2_L,$$

$$|\Sigma_c \bar{D}^*(1/2^-)\rangle = \frac{1}{2\sqrt{3}} 0_H \otimes 1/2_L + \frac{5}{6} 1_H \otimes 1/2_L - \frac{\sqrt{2}}{3} 1_H \otimes 3/2_L,$$

$$|\Sigma_c \bar{D}^*(3/2^-)\rangle = \frac{1}{\sqrt{3}} 0_H \otimes 3/2_L - \frac{1}{3} 1_H \otimes 1/2_L + \frac{\sqrt{5}}{3} 1_H \otimes 3/2_L,$$

$$|\Sigma_c^*\bar{D}^*(1/2^-)\rangle = \sqrt{\frac{2}{3}}0_H \otimes 1/2_L - \frac{\sqrt{2}}{3}1_H \otimes 1/2_L - \frac{1}{3}1_H \otimes 3/2_L,$$
$$|\Sigma_c^*\bar{D}^*(3/2^-)\rangle = \frac{\sqrt{\frac{5}{3}}}{2}0_H \otimes 3/2_L + \frac{\sqrt{5}}{3}1_H \otimes 1/2_L - \frac{1}{6}1_H \otimes 3/2_L. \quad \text{(A2)}$$

The total light quark spin $1/2_L$ of the $\bar{D}^{(*)}\Sigma_c^{(*)}$ system is given by the coupling of the light quark spins, $1/2_{1l} \otimes 1_{2l}$. Since the light quark spin of Λ_c is 0, the total light quark spin $1/2'_L$ of the $\bar{D}^{(*)}\Lambda_c$ system is given by $1/2_{1l} \otimes 0_{2l}$. The decompositions of the $\bar{D}^{(*)}\Lambda_c$ states are written as

$$|\bar{D}\Lambda_c(J^P = 1/2^-)\rangle = -\frac{1}{2}0_H \otimes 1/2'_L + \frac{\sqrt{3}}{2}1_H \otimes 1/2'_L,$$
$$|\bar{D}^*\Lambda_c(J^P = 1/2^-)\rangle = \frac{\sqrt{3}}{2}0_H \otimes 1/2'_L + \frac{1}{2}1_H \otimes 1/2'_L,$$
$$|\bar{D}^*\Lambda_c(J^P = 3/2^-)\rangle = 1_H \otimes 1/2'_L. \quad \text{(A3)}$$

In the heavy quark limit, the $\bar{D}^{(*)}\Sigma_c^{(*)} \to \bar{D}^{(*)}\Sigma_c^{(*)}$ interactions are independent of the spin of the heavy quark, and therefore the potentials can be parametrized by two coupling constants describing the interactions between light quarks of spin 1/2 and 3/2, respectively, i.e., $F_{1/2} = \langle 1/2_L|V|1/2_L\rangle$ and $F_{3/2} = \langle 3/2_L|V|3/2_L\rangle$:

$$V_{\Sigma_c\bar{D}}(1/2^-) = \frac{1}{3}F_{1/2L} + \frac{2}{3}F_{3/2L},$$
$$V_{\Sigma_c^*\bar{D}}(3/2^-) = \frac{1}{3}F_{1/2L} + \frac{2}{3}F_{3/2L},$$
$$V_{\Sigma_c\bar{D}^*}(1/2^-) = \frac{7}{9}F_{1/2L} + \frac{2}{9}F_{3/2L},$$
$$V_{\Sigma_c\bar{D}^*}(3/2^-) = \frac{1}{9}F_{1/2L} + \frac{8}{9}F_{3/2L},$$
$$V_{\Sigma_c^*\bar{D}^*}(1/2^-) = \frac{8}{9}F_{1/2L} + \frac{1}{9}F_{3/2L},$$
$$V_{\Sigma_c^*\bar{D}^*}(3/2^-) = \frac{5}{9}F_{1/2L} + \frac{4}{9}F_{3/2L}. \quad \text{(A4)}$$

which can be rewritten as a combination of C_a and C_b, i.e., $F_{1/2} = C_a - 2C_b$ and $F_{3/2} = C_a + C_b$ [63].

In the heavy quark limit, the $\bar{D}^{(*)}\Lambda_c \to \bar{D}^{(*)}\Lambda_c$ interactions are parametrized by one coupling constant, i.e., $F'_{1/2L} = \langle 1/2'_L|V|1/2'_L\rangle$:

$$V_{\bar{D}\Lambda_c}(1/2^-) = V_{\bar{D}^*\Lambda_c}(1/2^-) = V_{\bar{D}^*\Lambda_c}(3/2^-) = F'_{1/2L}, \quad \text{(A5)}$$

where the parameter $F'_{1/2L}$ can be rewritten as C'_a.

The potentials of $J/\psi N \to J/\psi N$, $J/\psi N \to \eta_c N$ and $\eta_c N \to \eta_c N$ are suppressed due to the Okubo-Zweig-Iizuka (OZI) rule, which is also supported by lattice QCD simulations [107]. In this work, we set $V_{J/\psi(\eta_c)N\to J/\psi(\eta_c)N} = 0$.

In the heavy quark limit, the $\bar{D}^{(*)}\Sigma_c^{(*)} \to J/\psi(\eta_c)N$ and $\bar{D}^{(*)}\Sigma_c^{(*)} \to J/\psi\Delta$ potentials are allowed, while the $\bar{D}^{(*)}\Sigma_c^{(*)} \to J/\psi\Delta$ potentials are suppressed due to isospin symmetry breaking. From HQSS, the $\bar{D}^{(*)}\Sigma_c^{(*)} \to J/\psi(\eta_c)N$ interactions are only related to the spin of the light quark 1/2, denoted by one coupling: $g_2 = \langle \bar{D}^{(*)}\Sigma_c^{(*)}|1_H \otimes 1/2_L\rangle = \langle \bar{D}^{(*)}\Sigma_c^{(*)}|0_H \otimes 1/2_L\rangle$. Similarly, we can express the $\bar{D}^{(*)}\Lambda_c \to J/\psi(\eta_c)N$ interactions by another parameter: $g_1 = \langle \bar{D}^{(*)}\Lambda_c|1_H \otimes 1/2_L\rangle = \langle \bar{D}^{(*)}\Lambda_c|0_H \otimes 1/2_L\rangle$. As for the $\bar{D}^{(*)}\Sigma_c^{(*)} \to \bar{D}^{(*)}\Lambda_c$ interactions, they are dependent on only one coupling constant in the heavy quark limit. Therefore, we parametrize the $\bar{D}^{(*)}\Sigma_c^{(*)} \to \bar{D}^{(*)}\Lambda_c$ potential by one coupling: $C'_b = \langle \bar{D}^{(*)}\Sigma_c^{(*)}|\bar{D}^{(*)}\Lambda_c\rangle$.

In the heavy quark limit, the contact-range potentials of $\bar{D}^*\Sigma_c^* - \bar{D}^*\Sigma_c - \bar{D}\Sigma_c - \bar{D}^*\Lambda_c - \bar{D}\Lambda_c - J/\psi N - \eta_c N$ system with $J^P = 1/2^-$ can be expressed as

$$V^{J=1/2} = \begin{pmatrix} C_a - \frac{5}{3}C_b & -\frac{\sqrt{2}}{3}C_b & -\sqrt{\frac{2}{3}}C_b & \sqrt{\frac{2}{3}}C'_b & \sqrt{2}C'_b & -\frac{\sqrt{2}}{3}g_2 & \sqrt{\frac{2}{3}}g_2 \\ -\frac{\sqrt{2}}{3}C_b & C_a - \frac{4}{3}C_b & \frac{2}{\sqrt{3}}C_b & -\frac{2}{\sqrt{3}}C'_b & C'_b & \frac{5}{6}g_2 & \frac{1}{2\sqrt{3}}g_2 \\ -\sqrt{\frac{2}{3}}C_b & \frac{2}{\sqrt{3}}C_b & C_a & C'_b & 0 & \frac{1}{2\sqrt{3}}g_2 & \frac{1}{2}g_2 \\ \sqrt{\frac{2}{3}}C'_b & -\frac{2}{\sqrt{3}}C'_b & C'_b & C'_a & 0 & \frac{1}{2}g_1 & \frac{\sqrt{3}}{2}g_1 \\ \sqrt{2}C'_b & C'_b & 0 & 0 & C'_a & \frac{\sqrt{3}}{2}g_1 & -\frac{1}{2}g_1 \\ -\frac{\sqrt{2}}{3}g_2 & \frac{5}{6}g_2 & \frac{1}{2\sqrt{3}}g_2 & \frac{1}{2}g_1 & \frac{\sqrt{3}}{2}g_1 & 0 & 0 \\ \sqrt{\frac{2}{3}}g_2 & \frac{1}{2\sqrt{3}}g_2 & \frac{1}{2}g_2 & \frac{\sqrt{3}}{2}g_1 & -\frac{1}{2}g_1 & 0 & 0 \end{pmatrix} \quad \text{(A6)}$$

and the contact potentials of $\bar{D}^*\Sigma_c^* - \bar{D}^*\Sigma_c - \bar{D}\Sigma_c^* - \bar{D}^*\Lambda_c - J/\psi N$ system with $J^P = 3/2^-$ are written as

$$V^{J=3/2} = \begin{pmatrix} C_a - \frac{2}{3}C_b & -\frac{\sqrt{5}}{3}C_b & \sqrt{\frac{5}{3}}C_b & \sqrt{\frac{5}{3}}C_b' & \frac{\sqrt{5}}{3}g_2 \\ -\frac{\sqrt{5}}{3}C_b & C_a + \frac{2}{3}C_b & \frac{1}{\sqrt{3}}C_b & \frac{1}{\sqrt{3}}C_b' & -\frac{1}{3}g_2 \\ \sqrt{\frac{5}{3}}C_b & \frac{1}{\sqrt{3}}C_b & C_a & -C_b' & \frac{1}{\sqrt{3}}g_2 \\ \sqrt{\frac{5}{3}}C_b' & \frac{1}{\sqrt{3}}C_b' & -C_b' & C_a' & g_1 \\ \frac{\sqrt{5}}{3}g_2 & -\frac{1}{3}g_2 & \frac{1}{\sqrt{3}}g_2 & g_1 & 0 \end{pmatrix} \tag{A7}$$

APPENDIX B: LIGHT MESON SATURATION

Following Ref. [95], we expect the EFT couplings $C_a(C_a')$ and $C_b(C_b')$ to be saturated by scalar and vector meson exchanges

$$C_a^{\mathrm{sat}(\prime)}(\Lambda \sim m_\sigma, m_V) \propto C_a^S + C_a^V, \tag{B1}$$

$$C_b^{\mathrm{sat}(\prime)}(\Lambda \sim m_\sigma, m_V) \propto C_b^V. \tag{B2}$$

The value of the saturated couplings is expected to be proportional to the light meson M potential $V_M(\vec{q})$ at $|\vec{q}| = 0$ once we have removed the Dirac-delta term [95]. According to the one-boson exchange (OBE) model, the σ and $\rho(\omega)$ exchanges are responsible for the $\bar{D}^{(*)}\Sigma_c^{(*)} \to \bar{D}^{(*)}\Sigma_c^{(*)}$ potentials, while σ, ω exchanges and ρ exchange are allowed for the $\bar{D}^{(*)}\Lambda_c \to \bar{D}^{(*)}\Lambda_c$ potentials and $\bar{D}^{(*)}\Sigma_c^{(*)} \to \bar{D}^{(*)}\Lambda_c$ potentials due to isospin symmetry. This gives us [13]

$$C_a^{\mathrm{sat}(\sigma)}(\Lambda \sim m_\sigma) \propto -\frac{g_{\sigma 1} g_{\sigma 2}}{m_\sigma^2}, \tag{B3}$$

$$C_a^{\mathrm{sat}(V)}(\Lambda \sim m_\rho) \propto \frac{g_{V1} g_{V2}}{m_V^2}(1 + \vec{\tau}_1 \cdot \vec{T}_2), \tag{B4}$$

$$C_b^{\mathrm{sat}(V)}(\Lambda \sim m_\rho) \propto \frac{f_{V1} f_{V2}}{6M^2}(1 + \vec{\tau}_1 \cdot \vec{T}_2), \tag{B5}$$

$$C_a^{\mathrm{sat}(\sigma)\prime}(\Lambda \sim m_\sigma) \propto -\frac{g_{\sigma 1} g_{\sigma 3}}{m_\sigma^2}, \tag{B6}$$

$$C_a^{\mathrm{sat}(V)\prime}(\Lambda \sim m_\omega) \propto \frac{g_{V1} g_{V3}}{m_V^2}, \tag{B7}$$

$$C_b^{\mathrm{sat}(V)\prime}(\Lambda \sim m_\rho) \propto \frac{f_{V1} f_{V3}}{6M^2}(\vec{\tau}_1 \cdot \vec{t}_2), \tag{B8}$$

where $V = \rho, \omega$ and we have made the simplification that $m_\rho = m_\omega = m_V$. The proportionality constant is unknown and depends on the details of the renormalization process. In this work, we assume that these proportionality constants are the same. The g_{σ_1}, g_{σ_2}, and g_{σ_3} denote the couplings of the $\bar{D}^{(*)}$ mesons, $\Sigma_c^{(*)}$ baryons, and Λ_c baryon to the sigma meson, and g_{v1}, g_{v2}, and g_{v3} (f_{v1}, f_{v2}, and f_{v3}) denote the electric-type (magnetic-type) couplings between the $\bar{D}^{(*)}$ mesons, $\Sigma_c^{(*)}$ baryons, and Λ_c baryon and a light vector meson. M is a mass scale to render f_v dimensionless. Following Refs. [13,108], we tabulate the values of these couplings in Table X. The $\vec{\tau}_1 \cdot \vec{T}_2$ and $\vec{\tau}_1 \cdot \vec{t}_2$ are the isospin factors of $\bar{D}^{(*)}\Sigma_c^{(*)} \to \bar{D}^{(*)}\Sigma_c^{(*)}$ potentials and $\bar{D}^{(*)}\Sigma_c^{(*)} \to \bar{D}^{(*)}\Lambda_c$ potentials, which are $\vec{\tau}_1 \cdot \vec{T}_2 = -2$ and $\vec{\tau}_1 \cdot \vec{t}_2 = -\sqrt{3}$ for the total isospin $I = 1/2$.

TABLE X. Couplings of the light mesons of the OBE model (σ, ρ, ω) to the heavy-meson and heavy-baryon. For the magnetic-type coupling of the ρ and ω vector mesons we have used the decomposition $f_V = \kappa_V g_V$, with $V = \rho, \omega$. $M = 940$ MeV refers to the mass scale involved in the magnetic-type couplings [13,108].

Coupling	P/P^*	Coupling	Σ_Q/Σ_Q^*	Coupling	Λ_Q
$g_{\sigma 1}$	3.4	$g_{\sigma 2}$	6.8	$g_{\sigma 3}$	3.4
g_{v1}	2.6	g_{v2}	5.8	g_{v3}	2.9
κ_{v1}	2.3	κ_{v2}	1.7	κ_{v3}	1.2

[1] R. Aaij *et al.* (LHCb Collaboration), Phys. Rev. Lett. **115**, 072001 (2015).
[2] R. Aaij *et al.* (LHCb Collaboration), Phys. Rev. Lett. **122**, 222001 (2019).
[3] R. Aaij *et al.* (LHCb Collaboration), Phys. Rev. Lett. **128**, 062001 (2022).
[4] R. Aaij *et al.* (LHCb Collaboration), Sci. Bull. **66**, 1278 (2021).
[5] R. Aaij *et al.* (LHCb Collaboration), Phys. Rev. Lett. **131**, 031901 (2023).
[6] R. Chen, Z.-F. Sun, X. Liu, and S.-L. Zhu, Phys. Rev. D **100**, 011502 (2019).
[7] J. He, Eur. Phys. J. C **79**, 393 (2019).
[8] H.-X. Chen, W. Chen, and S.-L. Zhu, Phys. Rev. D **100**, 051501 (2019).
[9] C. W. Xiao, J. Nieves, and E. Oset, Phys. Rev. D **100**, 014021 (2019).
[10] S. Sakai, H.-J. Jing, and F.-K. Guo, Phys. Rev. D **100**, 074007 (2019).
[11] Y. Yamaguchi, H. García-Tecocoatzi, A. Giachino, A. Hosaka, E. Santopinto, S. Takeuchi, and M. Takizawa, Phys. Rev. D **101**, 091502 (2020).
[12] J. He and D.-Y. Chen, Eur. Phys. J. C **79**, 887 (2019).
[13] M.-Z. Liu, T.-W. Wu, M. Sánchez Sánchez, M. P. Valderrama, L.-S. Geng, and J.-J. Xie, Phys. Rev. D **103**, 054004 (2021).
[14] M. Pavon Valderrama, Phys. Rev. D **100**, 094028 (2019).
[15] L. Meng, B. Wang, G.-J. Wang, and S.-L. Zhu, Phys. Rev. D **100**, 014031 (2019).
[16] M.-L. Du, V. Baru, F.-K. Guo, C. Hanhart, U.-G. Meißner, J. A. Oller, and Q. Wang, Phys. Rev. Lett. **124**, 072001 (2020).
[17] X.-Z. Ling, J.-X. Lu, M.-Z. Liu, and L.-S. Geng, Phys. Rev. D **104**, 074022 (2021).
[18] X.-K. Dong, F.-K. Guo, and B.-S. Zou, Prog. Phys. **41**, 65 (2021).
[19] U. Özdem, Eur. Phys. J. C **81**, 277 (2021).
[20] Y.-W. Pan, T.-W. Wu, M.-Z. Liu, and L.-S. Geng, Phys. Rev. D **105**, 114048 (2022).
[21] Z. Zhang, J. Liu, J. Hu, Q. Wang, and U.-G. Meißner, Sci. Bull. **68**, 981 (2023).
[22] Y.-W. Pan, T.-W. Wu, M.-Z. Liu, and L.-S. Geng, Eur. Phys. J. C **82**, 908 (2022).
[23] Z.-W. Liu, J.-X. Lu, M.-Z. Liu, and L.-S. Geng, Phys. Rev. D **108**, L031503 (2023).
[24] M. I. Eides, V. Y. Petrov, and M. V. Polyakov, Mod. Phys. Lett. A **35**, 2050151 (2020).
[25] A. Ali and A. Y. Parkhomenko, Phys. Lett. B **793**, 365 (2019).
[26] Z.-G. Wang, Int. J. Mod. Phys. A **35**, 2050003 (2020).
[27] J.-B. Cheng and Y.-R. Liu, Phys. Rev. D **100**, 054002 (2019).
[28] X.-Z. Weng, X.-L. Chen, W.-Z. Deng, and S.-L. Zhu, Phys. Rev. D **100**, 016014 (2019).
[29] R. Zhu, X. Liu, H. Huang, and C.-F. Qiao, Phys. Lett. B **797**, 134869 (2019).
[30] A. Pimikov, H.-J. Lee, and P. Zhang, Phys. Rev. D **101**, 014002 (2020).
[31] W. Ruangyoo, K. Phumphan, C.-C. Chen, A. Limphirat, and Y. Yan, J. Phys. G **49**, 075001 (2022).
[32] C. Fernández-Ramírez, A. Pilloni, M. Albaladejo, A. Jackura, V. Mathieu, M. Mikhasenko, J. A. Silva-Castro, and A. P. Szczepaniak (JPAC Collaboration), Phys. Rev. Lett. **123**, 092001 (2019).
[33] S. X. Nakamura, Phys. Rev. D **103**, L111503 (2021).
[34] T. J. Burns and E. S. Swanson, Phys. Rev. D **106**, 054029 (2022).
[35] J.-M. Xie, X.-Z. Ling, M.-Z. Liu, and L.-S. Geng, Eur. Phys. J. C **82**, 1061 (2022).
[36] Y.-H. Lin, C.-W. Shen, F.-K. Guo, and B.-S. Zou, Phys. Rev. D **95**, 114017 (2017).
[37] T. J. Burns and E. S. Swanson, Eur. Phys. J. A **58**, 68 (2022).
[38] Z. E. Meziani *et al.*, arXiv:1609.00676.
[39] A. Ali *et al.* (GlueX Collaboration), Phys. Rev. Lett. **123**, 072001 (2019).
[40] X. Cao and J.-p. Dai, Phys. Rev. D **100**, 054033 (2019).
[41] Q. Wang, X.-H. Liu, and Q. Zhao, Phys. Rev. D **92**, 034022 (2015).
[42] A. N. Hiller Blin, C. Fernández-Ramírez, A. Jackura, V. Mathieu, V. I. Mokeev, A. Pilloni, and A. P. Szczepaniak, Phys. Rev. D **94**, 034002 (2016).
[43] M. Karliner and J. L. Rosner, Phys. Lett. B **752**, 329 (2016).
[44] X.-Y. Wang, X.-R. Chen, and J. He, Phys. Rev. D **99**, 114007 (2019).
[45] J.-J. Wu, T. S. H. Lee, and B.-S. Zou, Phys. Rev. C **100**, 035206 (2019).
[46] S.-Y. Li, Y.-R. Liu, Y.-N. Liu, Z.-G. Si, and X.-F. Zhang, Commun. Theor. Phys. **69**, 291 (2018).
[47] M. B. Voloshin, Phys. Rev. D **99**, 093003 (2019).
[48] C.-h. Chen, Y.-L. Xie, H.-g. Xu, Z. Zhang, D.-M. Zhou, Z.-L. She, and G. Chen, Phys. Rev. D **105**, 054013 (2022).
[49] P. Ling, X.-H. Dai, M.-L. Du, and Q. Wang, Eur. Phys. J. C **81**, 819 (2021).
[50] P.-P. Shi, F.-K. Guo, and Z. Yang, Phys. Rev. D **106**, 114026 (2022).
[51] E. Braaten, M. Kusunoki, and S. Nussinov, Phys. Rev. Lett. **93**, 162001 (2004).
[52] E. Braaten and M. Kusunoki, Phys. Rev. D **71**, 074005 (2005).
[53] M.-L. Du, V. Baru, F.-K. Guo, C. Hanhart, U.-G. Meißner, J. A. Oller, and Q. Wang, J. High Energy Phys. 08 (2021) 157.
[54] L. Roca, J. Nieves, and E. Oset, Phys. Rev. D **92**, 094003 (2015).
[55] Q. Wang, C. Hanhart, and Q. Zhao, Phys. Rev. Lett. **111**, 132003 (2013).
[56] F.-K. Guo, C. Hanhart, U.-G. Meißner, Q. Wang, and Q. Zhao, Phys. Lett. B **725**, 127 (2013).
[57] Y.-K. Hsiao, Y. Yu, and B.-C. Ke, Eur. Phys. J. C **80**, 895 (2020).
[58] M.-Z. Liu, X.-Z. Ling, L.-S. Geng, E. Wang, and J.-J. Xie, Phys. Rev. D **106**, 114011 (2022).
[59] Q. Wu, M.-Z. Liu, and L.-S. Geng, arXiv:2304.05269.
[60] Q. Wu and D.-Y. Chen, Phys. Rev. D **100**, 114002 (2019).
[61] A. F. Falk and M. Neubert, Phys. Rev. D **47**, 2982 (1993).
[62] T. Gutsche, M. A. Ivanov, J. G. Körner, and V. E. Lyubovitskij, Phys. Rev. D **98**, 074011 (2018).

[63] M.-Z. Liu, Y.-W. Pan, F.-Z. Peng, M. Sánchez Sánchez, L.-S. Geng, A. Hosaka, and M. Pavon Valderrama, Phys. Rev. Lett. **122**, 242001 (2019).
[64] M. Pavon Valderrama, Phys. Rev. D **100**, 094028 (2019).
[65] Y.-H. Lin and B.-S. Zou, Phys. Rev. D **100**, 056005 (2019).
[66] N. Yalikun, Y.-H. Lin, F.-K. Guo, Y. Kamiya, and B.-S. Zou, Phys. Rev. D **104**, 094039 (2021).
[67] L.-L. Chau, Phys. Rep. **95**, 1 (1983).
[68] L.-L. Chau and H.-Y. Cheng, Phys. Rev. D **36**, 137 (1987); **39**, 2788(A) (1989).
[69] R. Molina, J.-J. Xie, W.-H. Liang, L.-S. Geng, and E. Oset, Phys. Lett. B **803**, 135279 (2020).
[70] H.-Y. Cheng, Phys. Rev. D **56**, 2799 (1997); **99**, 079901(E) (2019).
[71] A. Ali, G. Kramer, and C.-D. Lu, Phys. Rev. D **58**, 094009 (1998).
[72] H.-n. Li, C.-D. Lu, and F.-S. Yu, Phys. Rev. D **86**, 036012 (2012).
[73] M. Bauer, B. Stech, and M. Wirbel, Z. Phys. C **34**, 103 (1987).
[74] T. Gutsche, M. A. Ivanov, J. G. Körner, V. E. Lyubovitskij, P. Santorelli, and N. Habyl, Phys. Rev. D **91**, 074001 (2015); **91**, 119907(E) (2015).
[75] P. A. Zyla *et al.* (Particle Data Group Collaboration), Prog. Theor. Exp. Phys. **2020**, 083C01 (2020).
[76] R. C. Verma, J. Phys. G **39**, 025005 (2012).
[77] S. Aoki *et al.* (Flavour Lattice Averaging Group Collaboration), Eur. Phys. J. C **80**, 113 (2020).
[78] Y.-H. Chen, H.-Y. Cheng, B. Tseng, and K.-C. Yang, Phys. Rev. D **60**, 094014 (1999).
[79] H.-Y. Cheng and C.-W. Chiang, Phys. Rev. D **81**, 074021 (2010).
[80] C.-K. Chua, Phys. Rev. D **100**, 034025 (2019).
[81] J.-M. Xie, M.-Z. Liu, and L.-S. Geng, Phys. Rev. D **107**, 016003 (2023).
[82] R. S. Azevedo and M. Nielsen, Phys. Rev. C **69**, 035201 (2004).
[83] M. E. Bracco, A. Cerqueira, Jr., M. Chiapparini, A. Lozea, and M. Nielsen, Phys. Lett. B **641**, 286 (2006).
[84] Z. G. Wang and S. L. Wan, Phys. Rev. D **74**, 014017 (2006).
[85] Z.-H. Guo and J. Oller, Phys. Lett. B **793**, 144 (2019).
[86] T. Ji, X.-K. Dong, M. Albaladejo, M.-L. Du, F.-K. Guo, J. Nieves, and B.-S. Zou, Sci. Bull. **68**, 688 (2023).
[87] E. Oset and A. Ramos, Nucl. Phys. **A635**, 99 (1998).
[88] D. Jido, J. A. Oller, E. Oset, A. Ramos, and U. G. Meissner, Nucl. Phys. **A725**, 181 (2003).
[89] J.-J. Wu, R. Molina, E. Oset, and B. S. Zou, Phys. Rev. Lett. **105**, 232001 (2010).
[90] T. Hyodo and D. Jido, Prog. Part. Nucl. Phys. **67**, 55 (2012).
[91] V. R. Debastiani, J. M. Dias, W. H. Liang, and E. Oset, Phys. Rev. D **97**, 094035 (2018).
[92] J. A. Oller and E. Oset, Nucl. Phys. **A620**, 438 (1997); **A652**, 407(E) (1999).
[93] L. Roca, E. Oset, and J. Singh, Phys. Rev. D **72**, 014002 (2005).
[94] Q. X. Yu, R. Pavao, V. R. Debastiani, and E. Oset, Eur. Phys. J. C **79**, 167 (2019).
[95] F.-Z. Peng, M.-Z. Liu, M. Sánchez Sánchez, and M. Pavon Valderrama, Phys. Rev. D **102**, 114020 (2020).
[96] F.-Z. Peng, M. Sánchez Sánchez, M.-J. Yan, and M. Pavon Valderrama, Phys. Rev. D **105**, 034028 (2022).
[97] X.-K. Dong, F.-K. Guo, and B.-S. Zou, Commun. Theor. Phys. **73**, 125201 (2021).
[98] Z.-C. Yang, Z.-F. Sun, J. He, X. Liu, and S.-L. Zhu, Chin. Phys. C **36**, 6 (2012).
[99] M.-X. Duan, L. Qiu, X.-Z. Ling, and Q. Zhao, arXiv: 2303.13329.
[100] Y.-W. Pan, M.-Z. Liu, F.-Z. Peng, M. Sánchez Sánchez, L.-S. Geng, and M. Pavon Valderrama, Phys. Rev. D **102**, 011504 (2020).
[101] H. Xing, J. Liang, L. Liu, P. Sun, and Y.-B. Yang, arXiv: 2210.08555.
[102] C.-J. Xiao, Y. Huang, Y.-B. Dong, L.-S. Geng, and D.-Y. Chen, Phys. Rev. D **100**, 014022 (2019).
[103] C. W. Xiao, J. X. Lu, J. J. Wu, and L. S. Geng, Phys. Rev. D **102**, 056018 (2020).
[104] Y. Yamaguchi, Y. Abe, K. Fukukawa, and A. Hosaka, EPJ Web Conf. **204**, 01007 (2019).
[105] N. Isgur and M. B. Wise, Adv. Ser. Dir. High Energy Phys. **10**, 234 (1992).
[106] J. M. Flynn and N. Isgur, J. Phys. G **18**, 1627 (1992).
[107] U. Skerbis and S. Prelovsek, Phys. Rev. D **99**, 094505 (2019).
[108] Y.-R. Liu and M. Oka, Phys. Rev. D **85**, 014015 (2012).